Neuropharmacology 261 (2024) 110152

Contents lists available at ScienceDirect

Neuropharmacology

journal homepage: www.elsevier.com/locate/neuropharm

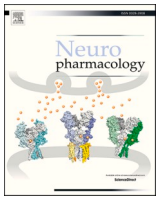

Minocycline mitigates Aβ and TAU pathology, neuronal dysfunction, and death in the PSEN1 E280A cholinergic-like neurons model of familial Alzheimer's disease

Daniela Giraldo-Berrio, Marlene Jimenez-Del-Rio **, Carlos Velez-Pardo *

Neuroscience Research Group, Institute of Medical Investigations, Faculty of Medicine, University of Antioquia (UdeA), Calle 70 No. 52-21, and Calle 62 # 52-59, Torre 1, Laboratory 412, Medellín, Colombia

ARTICLE INFO

Handling Editor: Prof F De Felice

Keywords:
Alzheimer's disease
Amyloid-beta
Apoptosis
Caspase 3
DJ-1
Hydrogen peroxide
Minocycline

ABSTRACT

Familial Alzheimer's disease (FAD) presenilin 1 E280A (PSEN1 E280A) is a severe neurological condition due to the loss of cholinergic neurons (ChNs), accumulation of amyloid beta (Aβ), and abnormal phosphorylation of the TAU protein. Up to date, there are no effective therapies available. The need for innovative treatments for this illness is critical. We found that minocycline (MC, 5 μM) was innocuous toward wild-type (WT) PSEN1 ChLNs but significantly (i) reduces the accumulation of intracellular Aβ by −69%, (ii) blocks both abnormal phosphorylation of the protein TAU at residue Ser202/Thr205 by −33% and (iii) phosphorylation of the proapoptotic transcription factor c-JUN at residue Ser63/Ser73 by −25%, (iv) diminishes oxidized DJ-1 at Cys106-SO_3 by −29%, (v) downregulates the expression of transcription factor TP53, (vi) BH-3-only protein PUMA, and (vii) cleaved caspase 3 (CC3) by −33, −86, and −78%, respectively, compared with untreated PSEN1 E280A ChLNs. Additionally, MC increases the response to ACh-induced Ca^{2+} influx by +92% in mutant ChLNs. Oxygen radical absorbance capacity (ORAC) and ferric ion-reducing antioxidant power (FRAP) analysis showed that MC might operate more efficiently as a hydrogen atom transfer agent than a single electron transfer agent. *In silico* molecular docking analysis predicts that MC binds with high affinity to Aβ (Vina Score −6.6 kcal/mol), TAU (VS -6.5 kcal/mol), and caspase 3 (VS -7.1 kcal/mol). Taken together, our findings suggest that MC demonstrates antioxidant, anti-amyloid, and anti-apoptosis activity and promotes physiological ACh-induced Ca^{2+} influx in PSEN1 E280A ChLNs. The MC has therapeutic potential for treating early-onset FAD.

1. Introduction

Familial Alzheimer's disease (FAD) is a chronic, progressive neurodegenerative disorder characterized by memory loss due to deterioration of the cholinergic neurons of the nucleus basalis of Meynert (Ch4) and medial septal nucleus (Ch1) (Liu et al., 2015; Teipel et al., 2024), deposition of extracellular amyloid beta (eAβ) plaques, i.e., eAβ1-42, and intracellular neurofibrillary tangles (NFTs) composed of abnormally phosphorylated TAU (p-TAU) (Acosta-Baena et al., 2011; Dinkel et al., 2020; Mendez, 2017; Trejo-Lopez et al., 2022). Most, if not all, of the AD cases presenting early-onset (EO) pertain to familial AD (FAD) are caused by mutation in at least three highly penetrant genes: the amyloid precursor protein (*APP*, >100 variants), presenilin (*PSEN*) 1 (*PSEN1*, 350 variants), and *PSEN* 2 (80 variants) (https://www.alzforum.org/mutations, accessed in May 2024). Accordingly, a large population with EOAD (mean age onset 49 years) was first discovered in the state of Antioquia, Colombia (Lopera, 1997), wherein a glutamic acid (Glu, E) to alanine (Ala, A) mutation at codon 280 (E280A) occurs in the *PSEN1* gene (Lalli et al., 2014). Although FAD PSEN1 E280A has been extensively studied (e.g., https://www.alzforum.org/mutations/psen1-e280a-paisa, accessed in May 2024) and pharmacological attempts have been made (Reiman et al., 2023), therapies against this kind of AD are urgently in need. Nonetheless, scientific awareness of the critical role played by the accumulation of intracellular Aβ (iAβ) and apoptosis has added another layer of complexity to FAD (Lauritzen et al., 2019; Takahashi et al., 2017; Takasugi et al., 2023; Volloch and Rits-Volloch, 2023a). Therefore, medications that lower iAβ levels given prior to the neuron being implicated in the apoptotic pathway would have therapeutic significance (Volloch and Rits-Volloch, 2023b). Consequently,

* Corresponding author.
** Corresponding author.
E-mail addresses: marlene.jimenez@udea.edu.co (M. Jimenez-Del-Rio), calberto.velez@udea.edu.co (C. Velez-Pardo).

https://doi.org/10.1016/j.neuropharm.2024.110152
Received 27 May 2024; Received in revised form 26 August 2024; Accepted 4 September 2024
Available online 7 September 2024

Abbreviations

Aβ	amyloid-beta
CASP3	caspase 3
ChLNs	cholinergic-like neurons
CC3	cleaved caspase 3
EGCG	epigallocatechin 3-gallate
eAβ	extracellular amyloid-beta
FAD	familial Alzheimer's disease
FRAP	ferric ion-reducing antioxidant power
E280A	glutamic acid 280 alanine
H2O2	hydrogen peroxide
iAβ	intracellular amyloid-beta
MSCs	mesenchymal stromal cells
MC	Minocycline
OS	oxidative stress
ORAC	oxygen radical absorbance capacity
PUMA	P53 up-regulated modulator of apoptosis
PHF	paired helical filament
p-TAU	phosphorylated TAU
PSEN1	presenilin 1
TP53	tumor protein 53
WT	wild-type

Table 1
List of antibodies used for immunocytochemistry and for flow cytometry.

Antibody	Dilution	Company Cat #
Differentiation Markers		
Goat anti-ChAT	1:200	Millipore cat# AB144P
Rabbit anti-VAChT	1:500	Sigma-Aldrich Cat# SAB4200559
Protein Aggregation Markers		
[a]Mouse anti-Amyloid βA4 clone 1E8	1:500	Millipore clone 1E8 cat# MABN639
Rabbit anti-total TAU	1:500	Sigma-Aldrich cat# T6402
[b]Mouse anti-phosphorylated TAU	1:500	Thermo Fisher Scientific cat# MN1020 (AT8)
Oxidative Stress Markers		
[c]Rabbit anti-oxidized DJ-1- ox (Cys106)DJ-1	1:500	Abcam cat# ab169520
Proapoptotic Markers		
Rabbit anti-PUMA	1:500	Abcam cat# ab-9643
Mouse anti-P53	1:500	Millipore cat# MA5-12453
[d]Goat anti-phospho-c-Jun	1:500	Santa Cruz cat# sc-16312
Rabbit anti-caspase-3	1:500	Millipore cat# AB3623
Secondary Antibodies		
DyLight 488 horse anti-rabbit	1:500	Vector laboratories DI 1088
DyLight 594 horse anti-rabbit	1:500	Vector laboratories DI 1094
DyLight 488 horse anti-goat	1:500	Vector laboratories DI 3088
DyLight 594 horse anti-goat	1:500	Vector laboratories DI 3094
DyLight 488 horse anti-Mouse	1:500	Vector laboratories DI 2488
DyLight 594 horse anti-Mouse	1:500	Vector laboratories DI 2594

[a] This monoclonal antibody is specific for the first 2 amino acids (i.e., Asp-Ala) of the Amyloid beta (Aβ) peptide amino terminus.
[b] This antibody is specific for phospho-TAU (Ser202/Thr205).
[c] This recombinant monoclonal antibody is specific for PARK7/DJ1 – Oxidized (Cys106-SO3).
[d] This monoclonal antibody is specific for phospho-c-Jun (Ser63/Ser73).

finding small (natural or synthetic) chemical agents that stop or slow down FAD has taken precedence in research. According to this perspective, it is suggested that drug repurposing might hasten the discovery of novel therapies for AD sufferers (Anderson et al., 2023; Grabowska et al., 2023; Padhi and Govindaraju, 2022).

Minocycline (MC, PubChem Compound CID: 54675783, molecular formula: C23H28ClN3O7) identified as (IUPAC Name) 4S,4aS,5aR,12aR) −4,7-bis(dimethylamino) −1,10,11,12a-tetrahydroxy-3,12-dioxo-4a,5,5a,6-tetrahydro -4H-tetracene-2-carboxamide) is a second-generation tetracycline antibiotic widely used for the treatment of bacterial infections (Brogden et al., 1975; Flamm et al., 2019; Shortridge et al., 2021). Interestingly, MC has shown a variety of biological actions that are independent of their anti-microbial activity, including anti-inflammatory, anti-oxidant, and anti-apoptotic activities (Garrido-Mesa et al., 2013a; 2013b). Therefore, MC appears as an ideal therapeutic molecule due to its unique features, involving fast and completely absorption with a long half-life of approximately 16 h, excellent tissue penetration, and 100% bioavailability (Macdonald et al., 1973); it is a highly lipophilic molecule able to cross the blood-brain barrier, promoting its accumulation in the central nervous system; it has shown antioxidant activity against oxidative and nitrosative stress by direct scavenging activity of the superoxide (O2.-) and hydroxyl (.OH) free radicals, and the non-free radical hydrogen peroxide (H2O2), and peroxynitrite (ONOO) (Kraus et al., 2005; Schildknecht et al., 2011; Kładna et al., 2012); it chelates divalent metals (e.g. Fe^{2+}), attenuating iron neurotoxicity (Chen-Roetling et al., 2009), and inhibits cell death signaling (Griffin et al., 2011). In line with these observations, several *in vivo* evidences have shown that MC might be of therapeutic use in AD (Garcez et al., 2017; Gholami Mahmoudian et al., 2023; Zhao et al., 2022), despite its clinical failure to ameliorate mild AD (Howard et al., 2020). This last observation suggests that MC should be therapeutically used at the earliest in the development of the disorder as it occurs in autosomal-dominant AD patients (e.g., PSEN1 E280A patients, Acosta-Baena et al., 2011). Although no data is yet available to confirm this assumption, the use of *in vitro* models carrying the E280A mutation (Frederiksen et al., 2019; Mendivil-Perez et al., 2023; Soto-Mercado et al., 2020; Vallejo-Diez et al., 2019), wherein the intracellular accumulation of Aβ (iAβ) is critical for the mechanism of neuronal cell death by apoptosis (Soto-Mercado et al., 2020) could advance our knowledge on this issue.

The purpose of the study was to determine if MC affects the Alzheimer's phenotype in an established *in vitro* model of FAD (Soto-Mercado et al., 2020). Here we showed that MC is a multi-target agent that can positively impact PSEN1 E280a ChLNs at reversing neuronal dysfunction. Our findings suggest that MC operates as an antioxidant, anti-amyloid, antiapoptotic, and restorative agent of Ca^{2+} ion influx.

2. Materials and methods

2.1. Transdifferentiation of mesenchymal stromal cells (MSCs) into cholinergic-like neurons (ChLNs)

To this end, wild-type (WT) and Wharton's umbilical cord jelly mesenchymal cells (WJ-MSCs) harboring the PSEN1 E280A mutation were differentiated according to previous methods (Mendivil-Perez et al., 2019). Briefly, WT MSCs PSEN1 (Tissue Bank Code # WJMSC-19) and PSEN1 E280A (TBC# WJMSC-24) were seeded at a density of 1–1.5 × 10^4 cells/cm^2 on laminin-coated culture plates in regular culture medium (RCm) for 24 h. Then, the cells were incubated in cholinergic differentiation medium (*Cholinergic-N-Run* medium, hereafter referred to as Ch-N-Rm) at 37 °C for 7 days. The neuronal cells were termed WT PSEN1 or PSEN1 E280A ChLNs and further cultured in regular culture medium (RCm) for an additional 4 days post-transdifferentiation.

2.2. Assay protocol

To determine whether MC (Sigma-Aldrich, cat #M9511) was

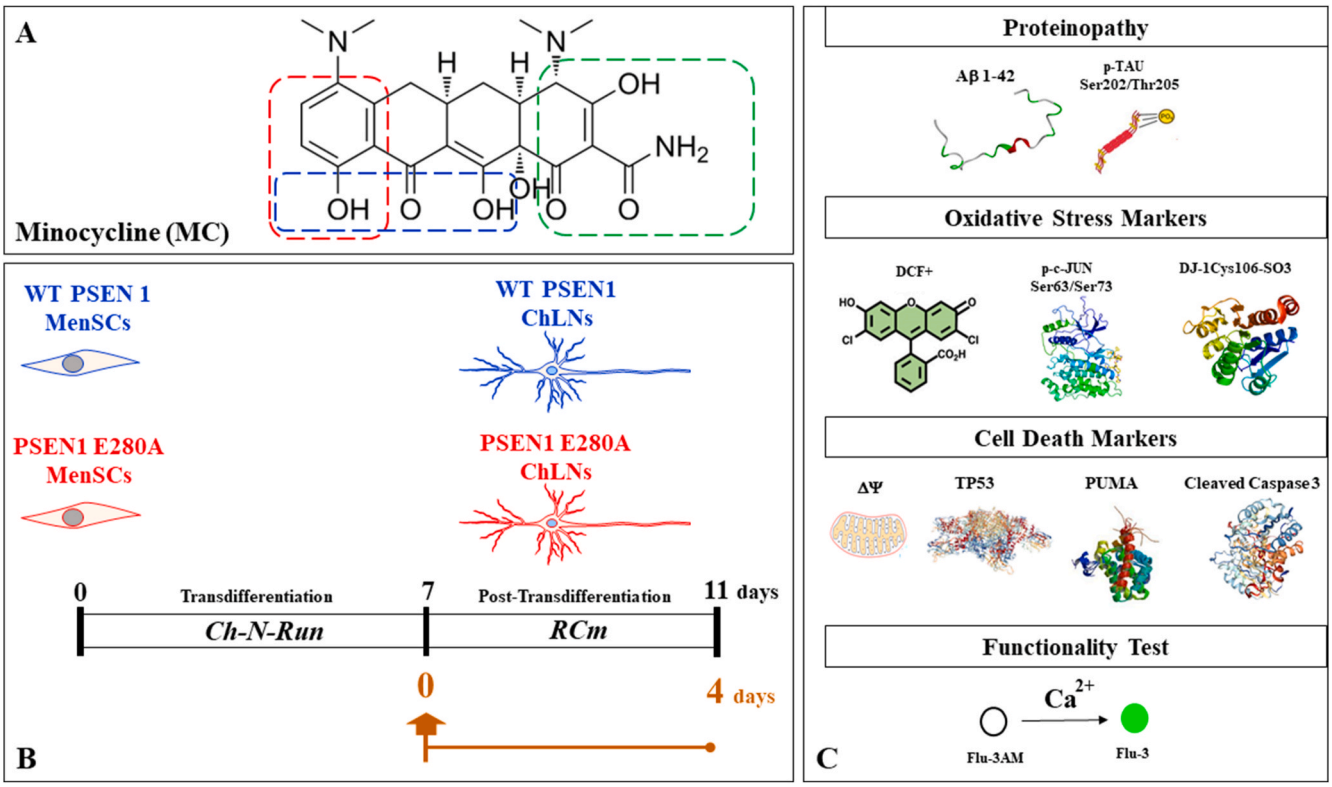

Fig. 1. Chemical structure, molecular formula of minocycline, schematic diagram of experimental procedure and molecular assays. (A) Minocycline (MC), PubChem Compound CID: 54675783, IUPAC Name: (4S,4aS,5aR,12aR)-4,7-bis(dimethylamino)-1,10,11,12a-tetrahydroxy-3,12-dioxo-4a,5,5a,6-tetrahydro-4H-tetracene-2-carboxamide, molecular formula (MF): $C_{23}H_{28}ClN_3O_7$. The red broken line represents site with direct antioxidative activity, the green broken line represents the site with poly(ADP-ribose) activity, and the blue broken line represents metal ion chelating. (B) Wild type (WT) or PSEN1 E280A menstrual stromal cells (MenSCs) cultured in Cholinergic-N-Run (Ch-N-R) medium for 7 days transdifferentiated into cholinergic-like neurons (ChLNs). Reagents were added at day 0 (day seven transdifferentiation), and left in culture in regular culture medium (RCm) for 4 additional days. (C) ChLNs were then evaluated for proteinopathy of disease such as accumulation of intracellular Aβ (i Aβ), phosphorylation p-TAU at Ser202/Thr205; oxidative stress (OS) (e.g., oxidation of DJ-1 at residue Cys106-SO3 and phosphorylation of c-JUN at Ser63/Ser73), cell death markers (e.g., loss of mitochondrial membrane potential (ΔΨm), overexpression of tumor protein 53 (TP53), p53 upregulated modulator of apoptosis (PUMA), cleaved caspase 3 (CC3)), and functionality test (e.g., acetyl choline (ACh)-induced Ca^{2+} ion influx).

cytotoxic, WT ChLNs were left untreated or exposed to increasing concentrations (1, 5, 10, 25 μM) of MC (n = 3). Given that the concentrations tested were innocuous to neurons, the pharmacological concentration of 5 μM MC was selected as the optimal concentration for further experiments. Accordingly, four groups of ChLNs were cultured: (i) untreated WT PSEN1, (ii) WT PSEN1 treated with MC (5 μM), (iii) untreated PSEN1 E280A, and (iv) PSEN1 E280A treated with MC (5 μM).

2.3. Immunofluorescence (IMF) and flow cytometry (FC) analyses

The cells were left untreated or treated with MC and assessed for several molecular markers using flow cytometry and fluorescence microscopy, the two most reliable techniques to analyze fluorescence-tagged proteins on a cell-by-cell basis (Costigan et al., 2023; Hollville and Martin, 2016). Proteinopathy, oxidative stress (OS), and cell death signaling markers were analyzed as previously described (Soto-Mercado et al., 2020). Briefly, cells treated under different conditions were processed by standard immunofluorescence protocols, which included primary antibodies and secondary fluorescent antibodies (Table 1). Nuclei were stained with 1 μM Hoechst 33342 (Life Technologies, 5791 Van Allen Way, Carlsbad, CA 92008, USA), and images were acquired using a Zeiss Axio Vert.A1 equipped with a Zeiss AxioCam Cm1 (Carl Zeiss Microscopy, LLC, One North Broadway, Floor 15 White Plains, NY 10601, United States). Fluorescence analysis was performed using a BD LSRFortessa II flow cytometer (BD Biosciences, Becton, Dickinson and Company, BD Biosciences, 2350 Qume Dr, San Jose, CA 95131-1812, USA). Cells incubated without primary antibodies were used as controls. For evaluation, 10,000 events and the quantitative data were obtained using FlowJo 7.6.2 data analysis software (TIBCO® Data Science Palo Alto, CA, USA). Event analysis was performed by determining the cell population (forward scatter analysis, Y-axis) that exceeded the baseline fluorescence (488 nm or 594 nm, X-axis) of the no primary antibody control. Consequently, contour/dot plots were created based on event analysis, and the cells located within the quadrant represented the cell population that exceeded the baseline fluorescence (Adan et al., 2017).

2.4. Molecular docking analysis

For molecular docking experiments, we employed the protein structure of monomeric Aβ (protein data bank code: 6SZF), TAU protein (Uniprot ID: P10636; PDB ID: 5O3L, 2ON9), and caspase-3 (PDB ID: 1NME) which were obtained using x-ray diffraction crystallography. CB-Dock version 2 (Liu et al., 2022), a cavity detection-guided protein-ligand blind docking online server that makes use of Autodock Vina (version 1.1.2, Scripps Research Institute, La Jolla, USA) was used to carry out the blind molecular docking. The SDF structure files of the tested compounds (minocycline, compound CID: 54675783; NSCI, compound CID: 11591540) was downloaded from PubChem (https://pubchem.ncbi.nlm.nih.gov/; accessed in May 2024). The molecular blind docking was performed by uploading the 3D structure PDB file of Aβ into the server with the SDF file of each compound. We chose the docking positions in the binding pocket that had the highest Vina score for study. The produced PDB files for the molecular docking of every

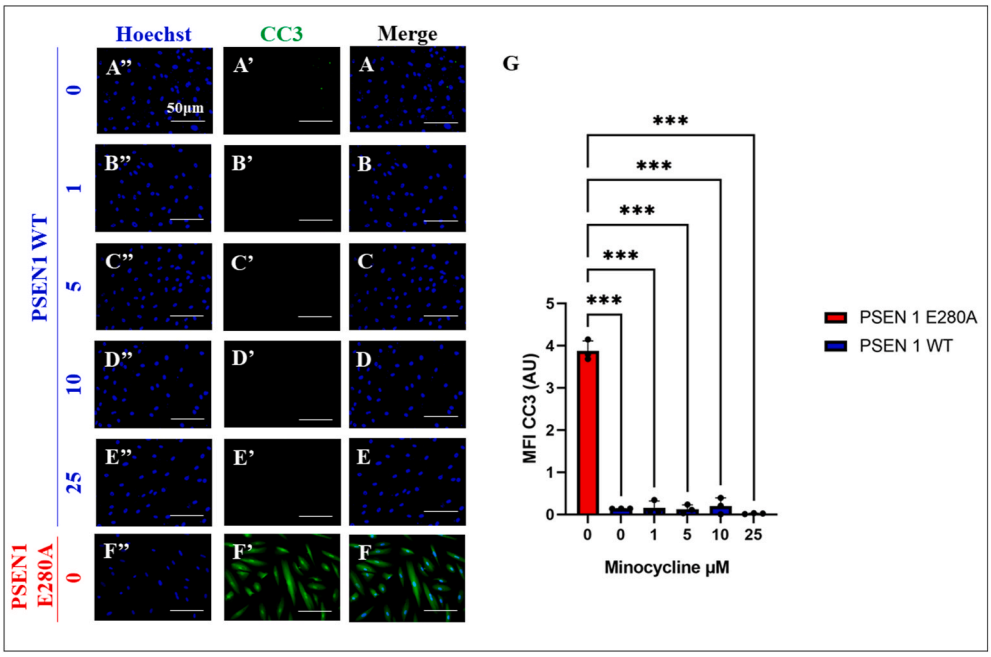

Fig. 2. Minocycline (MC) is innocuous to wild-type (WT) presenilin 1 (PSEN1) cholinergic-like neurons (ChLNs). Representative fluorescence microscopy merged images of (**A**) untreated WT ChLNs, or treated with MC (**B**) 1, (**C**) 5, (**D**) 10, and (**E**) 25 µM, or (**F**) untreated PSEN1 E280A ChLNs stained with antibodies against cleaved caspase 3 (CC3, A′-F′). Nuclei were stained with Hoechst (A″-F″). (**G**) Quantitative data showing the mean fluorescence intensity (MFI) of CC3. The figures represent 1 out of 3 independent experiments. The data are expressed as the mean ± standard deviation (SD); significant values were determined by one-way analysis of variance (ANOVA) test with Tukey's post hoc test. Statistical significance: ***$p < 0.001$.

compound were compared to the experimentally verified X-ray structures of the interaction between epigallocatechin 3-gallate (compound CID: 65064) and Aβ (Fang et al., 2022), TAU (Seidler et al., 2022), and caspase 3 (CASP3). These visualizations were made using the CB-Dock2 interphase or BIOVIA Discovery Studio Visualizer (https://discover.3ds.com/discovery-studio-visualizer-download; accessed in May 2024).

2.5. Intracellular calcium imaging

Changes in the intracellular calcium (Ca^{2+}) concentration induced by cholinergic stimulation were evaluated according to previous methods (Pap et al., 2009; Sekiguchi-Tonosaki et al., 2009), with minor modifications. The fluorescent dye Fluo-3 (Fluo-3 AM; Thermo Fisher Scientific, cat: F1242 168, Third Avenue, Waltham, MA, USA) was used for these measurements. The dye was dissolved in DMSO (1 mM) to form a stock solution. Prior to the experiments, the stock solution was diluted with neuronal buffer solution (NBS buffer (in mM): 137 NaCl, 5 KCl, 2.5 $CaCl_2$, 1 $MgCl_2$, pH 7.3, and 22 glucose). The working concentration of the dye was 2 µM. WT and PSEN1 E280A ChLNs were incubated for 30 min at 37 °C with dye-containing NBS buffer and then washed five times. Intracellular Ca^{2+} transients were evoked by acetylcholine (1 mM final concentration) 4 days after differentiation. Measurements were performed using the 20 × objective of the microscope. Several regions of interest (ROIs) were defined in the camera's visual field. One ROI was cell free, and the measured fluorescence intensity in this area was considered background fluorescence (F_{bg}). The time dependence of the fluorescence emission was determined, and the fluorescence intensities (thus, Ca^{2+} levels) were determined using pseudocolors. To calculate the changes in average fluorescence intensity related to Ca^{2+}, the F_{bg} value was determined from the cell-free ROI, and the resting fluorescence intensity (F_{rest}) of each of the ROIs containing cells was subsequently obtained as the average of the points recorded during a consecutive 10-s period prior to acetylcholine addition. Transient fluorescence peaks were identified by averaging six consecutive points and identifying those points that yielded the highest average value (F_{max}). The amplitudes of Ca^{2+}-related fluorescence transients were expressed relative to resting fluorescence (ΔF/F) and calculated using the following formula: $\Delta F/F = (F_{max} - F_{rest})/(F_{rest} - F_{bg})$. ImageJ was used for fluorescence intensity calculations. Fluorescence intensity was used as an indirect indicator of the intracellular Ca^{2+} concentration. This evaluation was repeated three times in independent blinded experiments.

2.6. Photomicrography and image analysis

Light and fluorescence microscopy images were taken using a Zeiss Axio Vert.A1 microscope connected to an AxioCam camera (Carl Zeiss Microscopy, LLC One North Broadway, Floor 15 White Plains, NY 10601, United States), according to previous methods (Soto-Mercado et al., 2020). The images were initially processed to remove background information using the Zen3.4 software (Zen Lite) function Background Subtraction to remove smooth backgrounds or correct uneven illumination. The implementation was adapted from the corresponding function in ImageJ and based on the rolling ball algorithm. Next, fluorescence images were analyzed using ImageJ software (http://imagej.nih.gov/ij/, accessed in May 2024). The figures were transformed into 8-bit images, and background subtraction was performed. Regions of interest (ROIs) were drawn around the nuclei (for transcription factors and apoptosis effectors) or around the cells in general (for cytoplasmic probes); subsequently, the fluorescence intensity was determined by applying the same threshold to the cells under control and treatment conditions. The mean fluorescence intensity (MFI) was obtained by normalizing the total fluorescence to the number of nuclei.

2.7. Oxygen radical absorbance capacity (ORAC) assay

The hydrophilic oxygen radical absorbance capacity (ORAC) assay was conducted following the protocol outlined in reference (Bravo et al., 2020). Essentially, a peroxyl radical generator, AAPH (2,2′-azobis (2-amidinopropane) dihydrochloride), a standard compound, Trolox, and a fluorescent probe, fluorescein, were employed. The ORAC values are reported as µmol Trolox equivalents (TE)/g of solution.

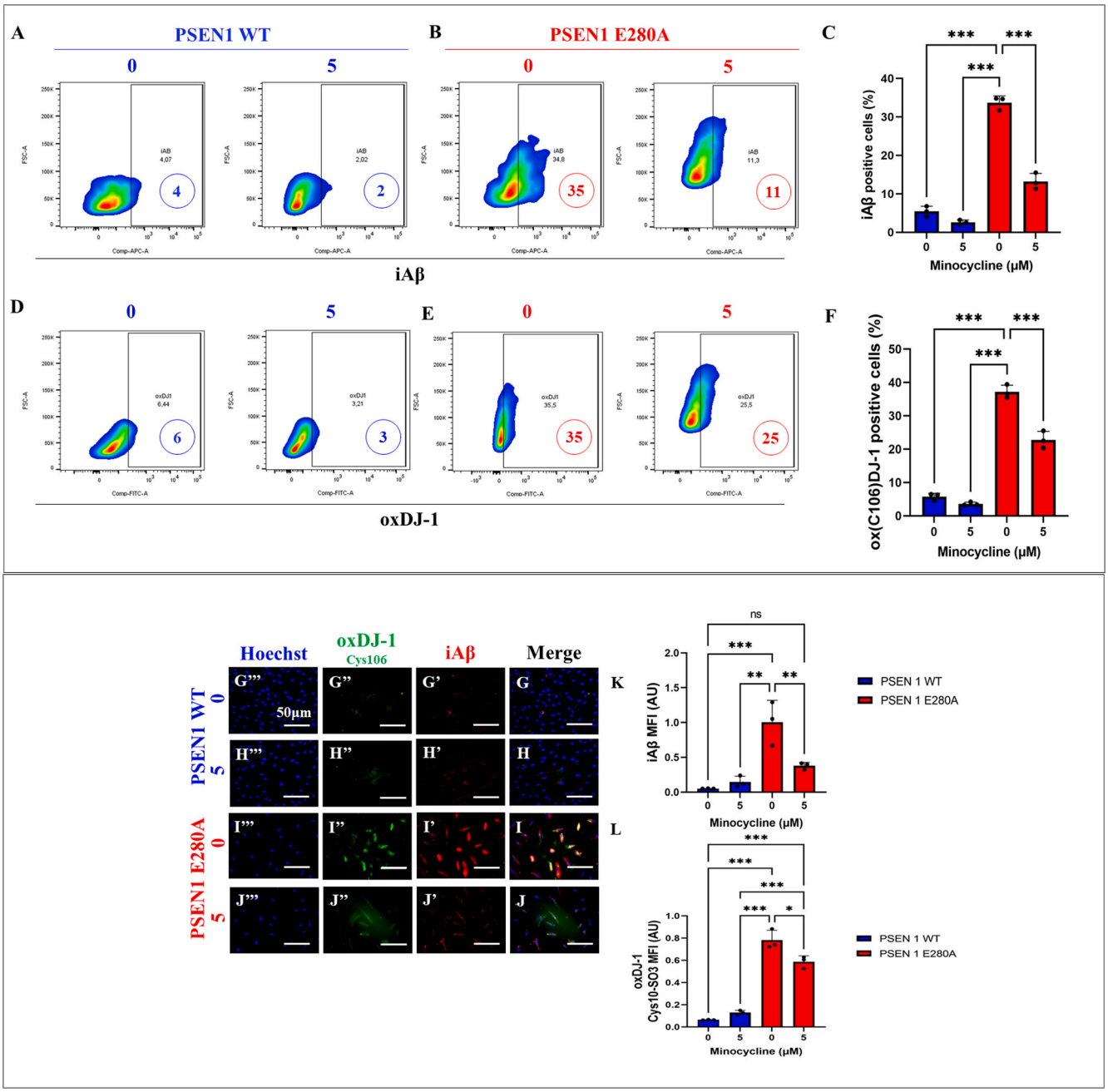

Fig. 3. Minocycline (MC) prevents the accumulation of intracellular Aβ (iAβ) and the oxidation of DJ-1 protein in PSEN1 E280A ChLNs. After 7 days of trans-differentiation, wild-type (WT) PSEN1 and E280A Cholinergic-like neurons (ChLNs) were left untreated or treated with MC (5 μM) in regular culture medium (RCm) for 4 days. (**A**) Flow cytometry (FC) density plots showing the percentage (number in circle) of iAβ in WT PSEN1 ChLNs and (**B**) iAβ in PSEN1 E280A ChLNs, (**C**) Quantification of the percentage of iAβ-positive cells, (**D**) FC density plots showing percentage (number in circle) of oxidized DJ-1 in WT PSEN1 ChLNs, (**E**) oxDJ-1 in PSEN1 E280A ChLNs, (**F**) Quantification of the percentage of oxDJ-1-positive cells. (**G-J**) Representative immunofluorescence merge images (**G-J**) showing WT PSEN1 and PSEN1 E280A ChLNs stained with antibodies against oxidized DJ-1 (G′–J′) and iAβ (G″–J″). Nuclei were stained with Hoechst (G‴–J‴). (**K**) Quantitative data showing the MFI of iAβ. (**L**) Quantitative data showing the mean fluorescence intensity (MFI) of oxDJ-1. Density plots and figures represent 1 of 3 independent experiments. Data are expressed as mean ± standard deviation (SD). Significant values were determined by one-way analysis of variance (ANOVA) test with Tukey's post hoc test. Statistical significance: *p < 0.05; **p < 0.01; ***p < 0.001.

2.8. Ferric reducing antioxidant power (FRAP) assay

The FRAP assay was performed as described previously (Bravo et al., 2020). Briefly, the samples and the working FRAP solution were mixed at a 1:25 ratio for 10 min of incubation at 37 °C in the dark. The FRAP values are expressed as μmol Trolox equivalents (TE)/g of solution (μmol TE/g).

2.9. Data analysis

In this experimental design, two vials of MSCs were thawed (WT PSEN1 and PSEN1 E280A), cultured and the cell suspension was pipetted at a standardized cellular density of 2.8 × 10^4 cells/cm^2 into different wells of a 24-well plate. Cells (i.e., the biological and observational unit (Lazic et al., 2018) were randomized to wells by simple randomization (sampling without replacement method), and then wells

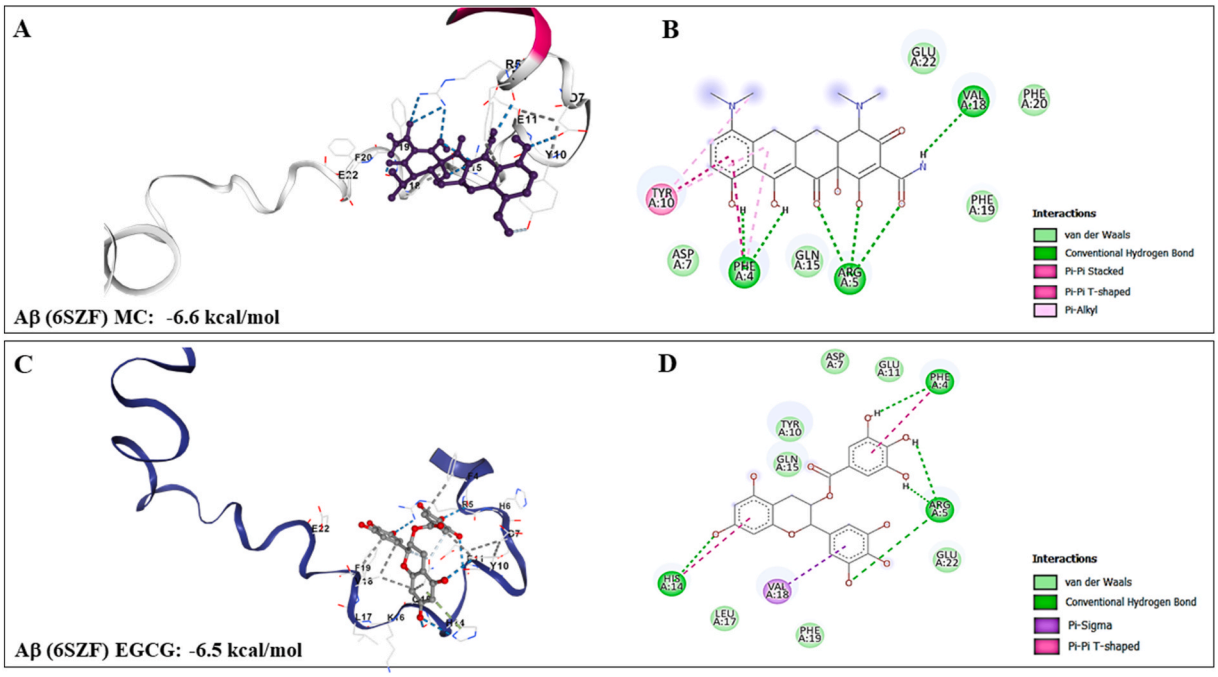

Fig. 4. *In silico* molecular docking analysis of the binding of MC and epigallocatechin 3-gallate (EGCG, used as reference molecule) to monomeric Aβ1-42. (**A**) Representative CB-Dock2 3D image showing the molecular docking of Aβ1-42 (PDB ID: 6SFZ) with MC (CID: 54675783); (**B**) 2D diagram showing conventional hydrogen bond between Aβ1-42-MC interaction, (**C**) Representative CB-Dock2 3D image showing the molecular docking of Aβ1-42 (ID: 6SFZ) with EGCG (CID: 65064); (**D**) 2D diagram showing conventional hydrogen bond between Aβ1-42-EGCG interaction.

(i.e., the experimental units) were randomized to treatments by a similar method. Experiments were performed on three independent occasions (n = 3) blind to the experimenter and/or flow cytometer analyst (Lazic et al., 2018). The data from the three repetitions i.e., independent experiments were averaged and a representative flow cytometry density or histogram plot from the three independent experiments was selected for illustrative purposes, whereas bar in quantification figures represent the mean ± SD and the three black dots show data point of each experimental repetition. Based on the assumption that the experimental unit (i.e., the well) data comply with the independence of observations, the dependent variable is normally distributed in each treatment group (Shapiro-Wilk test), and variances are homogeneous (Levene's test), the statistical significance was determined by one-way analysis of variance (ANOVA) followed by Tukey's post hoc comparison calculated with GraphPad Prism 5.0 software. Differences between groups were only deemed significant when a p-value of <0.05 (*), <0.001 (**) and <0.001 (***). All data are illustrated as the mean ± S.D. The ORAC and FRAP assays were performed once for each molecule (MC or EGCG >95%) in triplicated and the quantification was calculated using a calibration curve with Trolox standards of known concentrations. The results (mean ± SD) to ORAC and FRAP assays were expressed as μmol Trolox equivalent per g (μmol TE/g).

3. Results

3.1. Minocycline (MC) is a harmless treatment for wild-type (WT) cholinergic-like neurons (ChLNs) derived from Wharton's jelly mesenchymal stromal cells (WJ-MSCs)

We initially wanted to evaluate whether MC (Fig. 1A) affects the survival of ChLNs. To this end, WT ChLNs were exposed to increasing concentrations of MC (0, 1, 5, 10, or 25 μM) for 24 h at 37 °C (Fig. 1B), and cleaved caspase-3 (CC3) expression was evaluated as a marker of cell death by apoptosis (Fig. 1C–Jänicke et al., 1998). Fluorescence microscopy (FM) analysis shows ChLNs expressed no CC3-positive cells (Fig. 2A–E), indicating that MC did not induce apoptosis in ChLNs at the concentrations tested when compared to untreated neurons (Fig. 2G). PSEN1 E280A ChLNs, included as a positive control (Soto-Mercado et al., 2020), showed a significantly increased number of CC3+ cells (Fig. 2F and G). Given that there were no statistically significant differences between MC concentrations, we selected MC at low concentration (e.g., 5 μM) as the therapeutic pharmacological concentration for further experiments with PSEN1 E280A ChLNs.

3.2. Minocycline (MC) decreases the accumulation of intracellular aβ (iAβ), levels of oxidized DJ-1 at residue Cys106, and phosphorylated TAU at residues Ser202/Thr205 in PSEN1 E280A ChLNs

Previous data have shown that accumulated iAβ occurs simultaneously with oxidized DJ-1 Cys106-SO_3 and phosphorylated TAU in PSEN1 E280A ChLNs (Soto-Mercado et al., 2020). We next wanted to evaluate whether MC could diminish those neuropathological hallmarks in PSEN1 E280A ChLNs. Thus, WT and mutant ChLNs were left untreated or treated with MC (Fig. 1B). As shown in Fig. 3A and C, MC induced no important changes in the metabolic process of the amyloid precursor protein (APP) in WT, whereas significantly reducing the accumulation of i Aβ by −69% in mutant ChLNs (Fig. 3B) compared to untreated mutant cells (Fig. 3B and C) assessed by flow cytometry (FC) assay (Fig. 3A–C). Similar observations were obtained by fluorescence microscopy analysis (Fig. 3G–K). We further examined whether MC was capable of binding to Aβ (PDB: 6SZF, Santoro et al., 2021). *In silico* molecular docking analysis predicts that MC binds to a pocket of monomer Aβ42 composed of amino acid (AA) residues Phe4 Arg5 Asp7 Tyr10 Gln15 Val18 Phe19 Phe20 Glu22 (Fig. 4A and B, Table 2) with a high binding energy (Vina Score −6.6 kcal/mol) similar to the pocket of monomer Aβ42 bound by EGCG (Fig. 4C and D, Vina Score −6.5 kcal/mol), used as a control molecule (Table 2, Fang et al., 2022). Interestingly, MC interacts with 70% (7/10) hydrophobic AA of Aβ42 (Table 2) and with aa Phe4 Arg5 Val18 via conventional hydrogen bonds (Fig. 4B).

In parallel, we assessed whether MC abridged the oxidation of DJ-1 Cys106-SH (Kinumi et al., 2004). Flow cytometry analysis shows that

Table 2
In silico molecular docking analysis of Aβ single chain (PDB: **6SZF**), TAU single chain (Uniprot ID: **P10636**), TAU PHF6 (PDB: **2ON9**), TAU (4R–3R) AD PHF (PDB: **5O3L**), caspase 3 (PDB: **1NME**) with minocycline (MC), epigallocatechin 3-gallate (EGCG) or caspase 3 inhibitor NSCI as reference molecules (Fang et al., 2022; Seidler et al., 2022).

Submitted Protein PDB[a]	Submitted Ligand[b]	Vina Score[c]	Cavity volume (Å^3)	Center (x, y, z)	Docking size (x, y, z)	Contact residue
6SZF	Minocycline CID: 54675783	**−6.6**	9	−12, −4, 1	23, 23, 23	chain a: **Phe4 Arg5** Asp7 Tyr10 Gln15 **Val18** Phe19 Phe20 Glu22
	EGCG CID: 65064	**−6.5**	9	−12, −4, 1	23, 23, 23	chain a: **Phe4 Arg5** Asp7 Tyr10 Glu11 **His14** Gln15 Leu17 Val18 Phe19 Glu22
P10636	Minocycline CID: 54675783	**−6.5**	181	−38, −15, −19	23, 23, 23	chain a: Phe303 His304 Val305 Glu306 Ile307 Thr308 Asn310 Gln653 Val654 **Glu655** Val656 Lys657
	EGCG CID: 65064	**−6.9**	181	−38, −15, −19	23, 23, 23	chain a: Phe301 **Thr302** Phe303 **His304** Val305 Glu306 Val654 Glu655 Val656 **Lys657**
5O3L	Minocycline CID: 54675783	**−8.8**	496	190, 126, 143	23, 23, 23	chain c: His329 Lys331 chain d: Glu338 **Val339** Lys340 chain e: Asn327 His329 Lys331 chain f: Glu338 Val339 Lys340 chain g: Asn327 His329 Lys331 chain h: Glu338 Lys340 chain j: Glu338 **Lys340**
	EGCG CID: 65064	**−8.4**	496	190, 126, 143	23, 23, 23	chain b: Lys340 chain d: Glu338 **Val339** Lys340 chain e: His329 Lys331 chain f: Glu338 Val339 **Lys340** chain g: Asn327 His329 **Lys331** chain h: Glu338 Val339 Lys340 chain j: Glu338 Val339 Lys340
2ON9	Minocycline CID: 54675783	**−4.8**	0	1, −14, 6	23, 23, 23	chain a: Val306 **Gln307** Ile308 Tyr310 chain b:Val306 Gln307 Ile308 Val309 Tyr310
	EGCG CID: 65064	**−4.5**	0	1, −14, 6	23, 23, 23	chain a: **Gln307** Ile308 Val309 Tyr310 chain b: Val306 Gln307 Ile308
1NME	Minocycline CID: 54675783	**−7.1**	216	23, 118, 14	23, 23, 23	chain a: Met39 Met44 Thr77 Asn80 **Leu81** Lys82 chain b: **Leu223** Lys224 Gln225 Tyr226 Ala227 **Asp228** Lys229 Phe275 Tyr276 His277
	NSCI (conformer 11591540)	**−6.5**	216	23, 118, 14	23, 23, 23	chain a: Met44 Thr77 Asn80 Leu81 Lys82 chain b: Leu223 Lys224 Ala227 Asp228 Phe275 Tyr276 **His277**

Bold represents the amino acid of Aβ42, TAU, and CASP3 involved in the conventional hydrogen bonding with MC, EGCG and NSCI.
[a] According to RCSB Protein Data Base (https://www.rcsb.org/).
[b] According to PubChem database (https://pubchem.ncbi.nlm.nih.gov/).
[c] According to CB-dock2: An accurate protein-ligand bind cocking tool (https://cadd.labshare.cn/cb-dock2/php/index.php).

though MC did not affect the DJ-1 Cys106-SH status in WT ChLNs (Fig. 3D–F), it moderately reduced the oxidized DJ-1 Cys106-SO_3 marker from 35% (untreated) to 25% (treated cells), i.e., −29% (Fig. 3E and F). These observations were confirmed by fluorescence microscopy analysis (Fig. 3G–J, L). Given that MC is recognized as having antioxidant activity (Kładna et al., 2012; Kraus et al., 2005), we further investigated whether MC was able to perform hydrogen atom transfer and/or single electron transfer (HAT and SET, respectively) reactions *in vitro*. Effectively, MC was able to perform HAT and SET reactions, albeit with different strengths. MC displayed a (HAT)-based ORAC value of 49, 297.65 ± 3486.75 mmol TE/g, whereas it showed a (SET)-based FRAP value of 13,096.97 ± 83.63 mmol TE/g. For comparative purposes, we used the epigallocatechin-3-gallate (EGCG), a polyphenol amply used as reference molecule due to its known chemical structure (Nagle et al., 2006), biochemical effects, pharmacokinetic properties, as well as pharmacodynamic and physiological effects (Legeay et al., 2015; Kapoor et al., 2017), involving antioxidant activity (e.g., Song et al., 2022), anti-amylogenic (e.g., Andrich and Bieschke, 2015; Soto-Mercado et al., 2021, 2024), and anti-TAU aggregation agent (Guéroux et al., 2017). Therefore, EGCG used as a positive control displayed an ORAC value of 37,870.75 ± 671.43 mmol TE/g and a FRAP value of 28,350.29 ± 914.20 mmol TE/g. Interestingly, MC presented an increase of +30% HAT reaction but a reduction of −54% SET reaction over EGCG reactions. Accordingly, MC is driven to perform HAT rather than SET interactions.

We also assessed whether MC affects p-TAU and whether MC could bind to the protein TAU. As shown in Fig. 5, MC did not affect p-TAU (Ser202/Thr205) in WT ChLNs (Fig. 5A–C) but significantly reduced p-TAU (Ser202/Thr205) by −33% in PSEN1 E280A ChLNs (Fig. 5B and C) compared to untreated mutant cells (Fig. 5C). Similar results were obtained by fluorescence microscopy examination (Fig. 5D–H). To explore the possible interaction between MC and TAU, we used molecular docking analysis to predict the binding of MC with full-length monomeric TAU protein (Uniprot structure ID: P10636), the (4R–3R) AD paired helical filament (PHF, PDB structure: 5O3L; N-Term: Val306—C-Term: PHE378, (Pinzi et al., 2023), or with the third repeat structure (R3) insertion, namely PHF6, (Val306 Gln307 Ile308 Val309 Tyr310 Lys311, PDB: 2ON9, (Sawaya et al., 2007), which act as nucleation center of protein aggregation (von Bergen et al., 2000). Fig. 6 shows that MC binds with similar binding affinity to full-length TAU protein (Vina score (VS) −6.5 kcal/mol, Fig. 6A and B) compared to EGCG (VS -6.9 kcal/mol, Fig. 6C, D), a widely used small molecule in simulation models (Seidler et al., 2022). Interestingly, MC binds with a slightly higher binding affinity (VS -8.8 kcal/mol, Fig. 6E–G) to (4R–3R) AD PHF than EGCG (−8.4 kcal/mol, Fig. 6H–J). A similar trend was observed with regard to binding affinity of MC toward a much simpler TAU structure, PHF6 (VS -4.8 kcal/mol, Fig. 6K and L) when compared to EGCG (−4.5 kcal/mol, Fig. 6M and N, Table 2). Of note, MC and EGCG interact with similar AA at the binding pocket of the TAU protein (Fig. 6A–N, Table 2).

3.3. Minocycline (MC) decreases apoptosis markers in PSEN1 E280A ChLNs

Previously, it has shown that PSEN1 E280A ChLNs endogenously expressed apoptosis-related signaling molecules such as c-JUN, TP53, and CC3 (Soto-Mercado et al., 2020). We therefore sought to evaluate whether MC could decrease the activation of such signaling molecules in mutant ChLNs. As expected, MC was innocuous to WT ChLNs. Indeed,

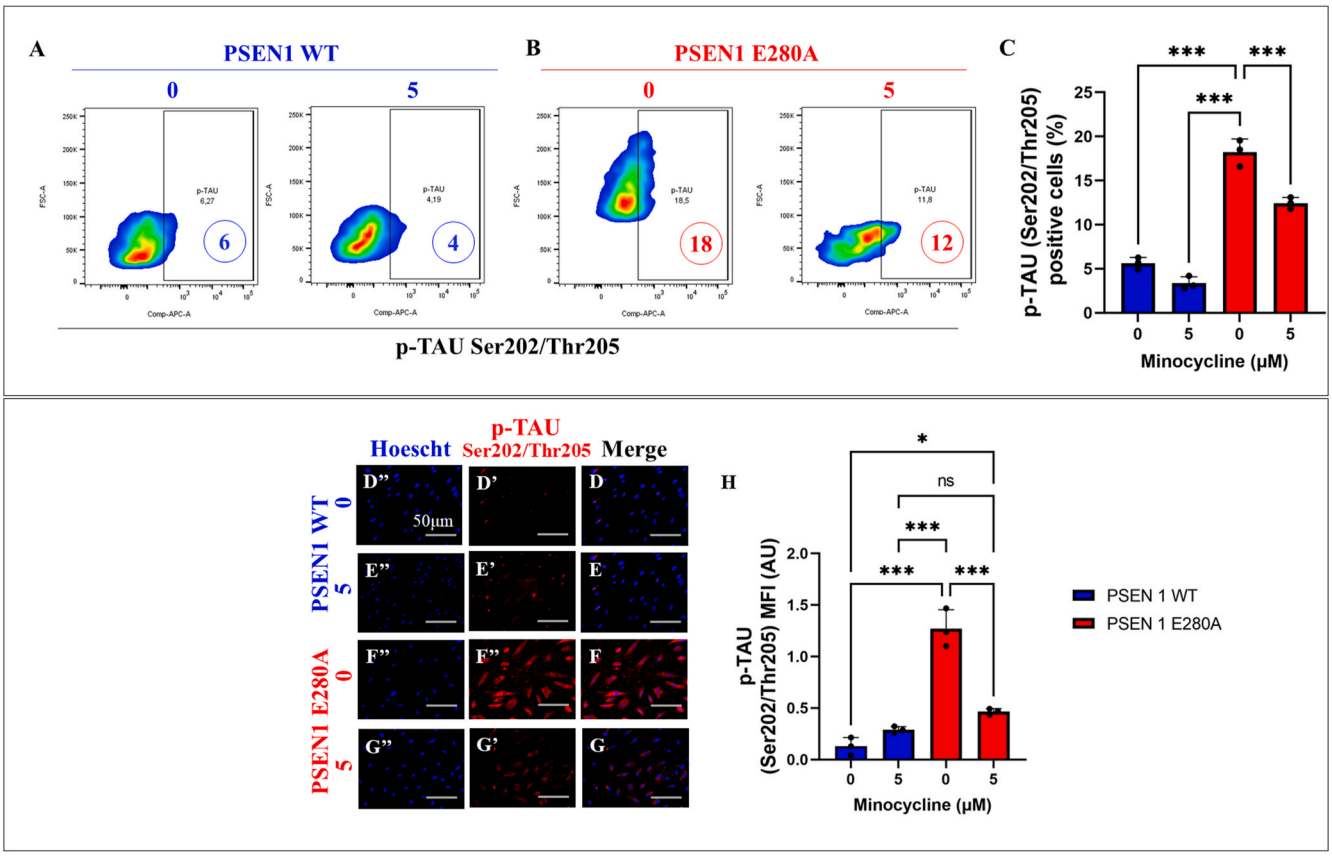

Fig. 5. Minocycline (MC) reduces phosphorylation of TAU (Ser202/Thr205) protein in PSEN1 E280A Cholinergic-like neurons (ChLNs). After 7 days of trans-differentiation, wild-type (WT) PSEN1 and E280A ChLNs were left untreated or treated with MC (5 μM) in regular culture medium (RCm) for 4 days. Flow cytometry (FC) density plots showing the percentage (number in circle) of p-TAU (Ser202/Thr205) in (**A**) WT PSEN1 ChLNs and (**B**) in PSEN1 E280A ChLNs, (**C**) Quantification of the percentage of p-TAU (Ser202/Thr205)-positive cells. Representative immunofluorescence merged images (**D-G**) showing WT PSEN1 and PSEN1 E280A ChLNs stained with antibodies against p-TAU (Ser202/Thr205) (D′-G′). Nuclei were stained with Hoechst (D″–G″). (**H**) Quantitative data showing the mean fluorescence intensity (MFI) of p-TAU (Ser202/Thr205). Density plots and figures represent 1 of 3 independent experiments. Data are expressed as mean ± standard deviation (SD). Significant values were determined by one-way analysis of variance (ANOVA) test with Tukey's post hoc test. Statistical significance: ***p < 0.001.

neither phosphorylation of c-JUN (Fig. 7A–C), expression of TP53 (Fig. 8A–C), PUMA (Fig. 8D–F), nor CC3+ cells (Fig. 9A–C) were observed in those cells. In contrast, compared to untreated mutant ChLNs, MC significantly reduced p-c-JUN Ser63/Ser73 by −25% (Fig. 7B and C), TP53 by −33% (Fig. 8B and C), PUMA (Fig. 8E and F) by −86%, and CC3+ by −78% (Fig. 9B and C) in PSEN1 ChLNs. These data were confirmed by fluorescence microscopy (Figs. 7D–H, 8G–L, 9D–H). Thus, we theoretically tested whether MC might bind to caspase-3 (CASP3). As a reference molecule, we used NSCI (1-(4-Methoxybenzyl)-5-[2-(pyridin-3-yl-oxymethyl)pyrrolidine-1-sulfonyl]-1H-indole-2,3-dione, PubChem CID 11591540, molecular weight 507.56, molecular formula C26H25N3O6S) -a nonpeptide CASP3 selective inhibitor (Chu et al., 2005). According to molecular docking evaluation, MC binds to a binding pocket of CASP3 with a higher binding affinity (Vina score −7.1 kcal/mol, Fig. 9I and J) than NSCI (Vina score −6.5 kcal/mol, Fig. 9K and L, Table 2).

3.4. Minocycline (MC) lessens dysfunctional Ca^{2+} ion influx in PSEN1 E280A ChLNs

We finally explored whether MC reverses dysfunctional Ca^{2+} influx in mutant ChLNs when they are stimulated with acetylcholine (ACh). WT and mutant ChLNs were cultured in the presence of ACh, after which cellular Ca^{2+} influx was analyzed via fluorescence microscopy. Fig. 10 shows that ACh induced a temporary elevation in intracellular Ca^{2+} in untreated WT neurons (Fig. 10A–E), but Ca^{2+} ion influx was even more stimulated in the presence of MC (Fig. 10B–E), according to Ca^{2+} response imaging (Fig. 10F). Remarkably, compared with untreated mutant ChLNs, which showed a decrease in ACh-induced Ca^{2+} influx (Fig. 10C–E, F), MC significantly increased the Ca^{2+} influx response (by a 1.91-fold increase) in ChLNs bearing the mutation E280A in PSEN1 (Fig. 10D, E, F).

4. Discussion

In the present investigation, we show that MC regressed the neuropathologic markers intrinsically produced by PSEN1 E280A ChLNs, i.e., accumulation of iAβ, OS, p-TAU, cell death, and ACh-induced Ca^{2+} influx dysfunction (Soto-Mercado et al., 2020). This action of MC on the mutant ChLNs might obey several mechanisms, including anti-amyloid, anti-oxidant, anti-TAU, anti-apoptotic, and ACh-induced Ca^{2+} influx enhancer. The following observations support that assumption. We found that MC efficiently reduced the accumulation of iAβ in mutated ChLNs by about −69% compared to untreated mutant cells (Fig. 3A–C). A possible explanation is that MC directly binds to the Aβ42 monomer, thereby interfering with the process of Aβ fibril formation, as previously shown in microglial cells (Familian et al., 2006). According to molecular binding analysis (Fig. 4A and B), similar to EGCG (Fang et al., 2022) (Fig. 4C and D). MC binds to a pocket of monomer Aβ with a high binding energy of -6.6 kcal/mol, involving the aromatic hydrophobic core region of Aβ42 (from Tyr10 to Phe20), which affects Aβ42 aggregation and can, consequently, disrupt interchain interactions in the Aβ42 protofibril structure and lead to the distortion of the protofibril structure and disassembly of Aβ (Firouzi et al., 2023). Briefly, the central

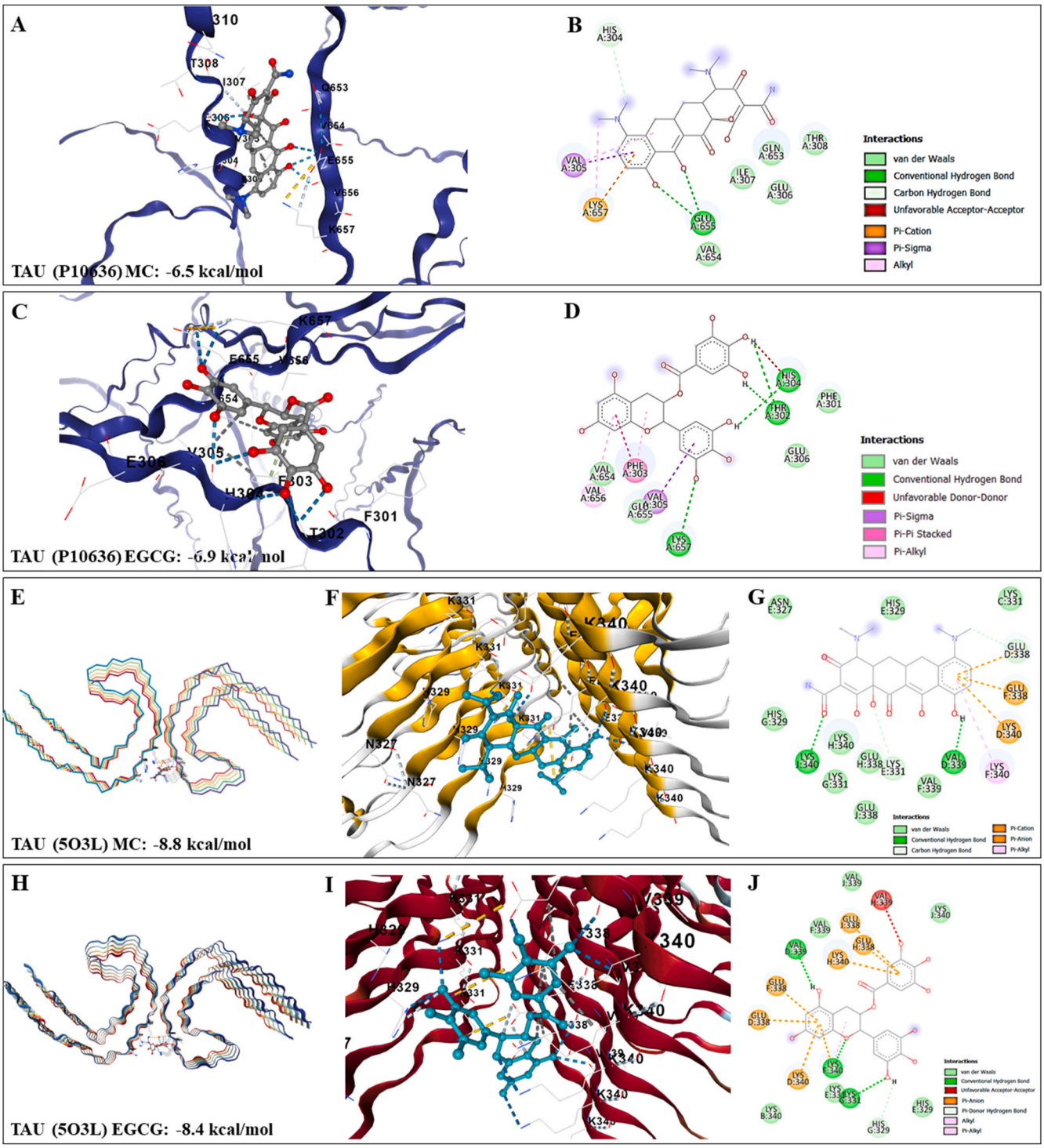

Fig. 6. *In silico* molecular docking analysis of the binding of MC and epigallocatechin 3-gallate (EGCG, used as reference molecule) to TAU protein. (**A**) Representative CB-Dock2 3D image showing the molecular docking of monomeric TAU (Uniprot ID: P10636) with MC (CID: 54675783); (**B**) 2D diagram showing conventional hydrogen bond between monomeric TAU-MC interaction, (**C**) Representative CB-Dock2 3D image showing the molecular docking of monomeric TAU with EGCG (CID: 65064); (**D**) 2D diagram showing conventional hydrogen bond between TAU-EGCG interaction. (**E**) Representative CB-Dock2 3D image showing the molecular docking of (4R–3R) AD PHF (PDB ID: 5O3L) with MC (CID: 54675783); (**F**) Closed-up of image in Fig. E, (**G**) 2D diagram showing conventional hydrogen bond between (4R–3R) AD PHF-MC interaction, (**H**) Representative CB-Dock2 3D image showing the molecular docking of (4R–3R) AD PHF with EGCG (CID: 65064); (**I**) Closed-up of image in Fig. H, (**J**) 2D diagram showing conventional hydrogen bond between (4R–3R) AD PHF-EGCG interaction; (**K**) Representative CB-Dock2 3D image showing the molecular docking of third repeat structure (R3) insertion, namely PHF6 (PDB ID: 2ON9) with MC (CID: 54675783); (**L**) 2D diagram showing conventional hydrogen bond between PHF6-MC interaction, (**M**) Representative CB-Dock2 3D image showing the molecular docking of PHF6 with EGCG (CID: 65064); (**N**) 2D diagram showing conventional hydrogen bond between PHF6-EGCG interaction.

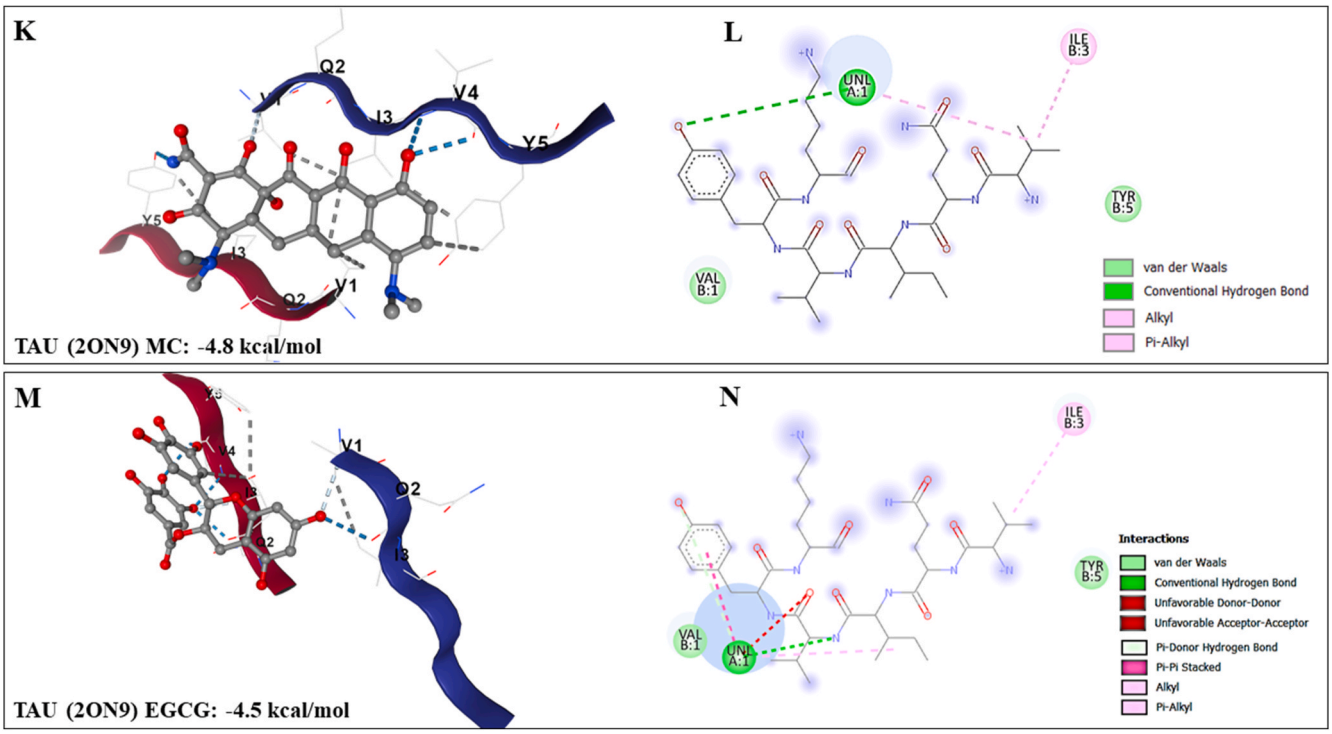

Fig. 6. (*continued*).

hydrophobic core (Leu17 Val18 Phe19 Phe20 Ala21) of the Aβ42 peptide shows dramatic changes under the influence of MC. In conclusion, MC can inhibit the conformational change of Aβ42 peptide (Hiroaki, 2023; Ngo et al., 2017) and delay the amyloidogenic potential of monomeric Aβ42 peptide (Doig and Derreumaux, 2015). Alternatively, MC may inhibit BACE-1, the β-secretase indispensable for the generation of Aβ42 (Ferretti et al., 2012). Whatever the mechanism, we show that MC significantly reduced the accumulation of iAβ (Fig. 3A–C, G'-J′, K). Therefore, MC is promising agent in inhibiting the misfolding conformation and self-assembly of Aβ42.

Similar to its anti-amyloid action, MC significantly reduced the oxidation of DJ-1 (Fig. 3D–F, G''-J″, L), resulting from the oxidation of residue Cys106-SH into Cys106-SO_3 (Kinumi et al., 2004). Effectively, MC has been shown to exhibit powerful free-radical scavenging activity (Kraus et al., 2005) due to its phenol ring structure (Fig. 1A, red broken line). Because of the resonance stabilization and steric hindrance surrounding the phenol group, free radicals have the ability to remove the hydrogen atom from the phenolic hydroxyl group in the MC molecule, producing a phenol-derived free radical that is significantly less reactive (Kraus et al., 2005). This agrees with MC displaying high (HAT)-based ORAC activity (this work). MC might also work by avoiding the oxidation of Cys106-SH, thereby maintaining this susceptible residue to oxidation in a reduced state. Taken together, these observations suggest that MC might exert antioxidant activity in PSEN1 E280A ChLNs against Aβ-induced OS due to its free scavenging activity or its reducing activity (Kładna et al., 2012; Kraus et al., 2005).

We report for the first time that MC diminished TAU pathology, i.e., p-TAU Ser202/SerThr205 (Fig. 5A–H). However, no data is available to explain this outcome. One possible explanation is that MC binds with high affinity to the TAU protein, according to molecular docking analysis (Fig. 6A, B, E-G, K, L). Similar to EGCG (Seidler et al., 2022) (Fig. 6C, D, H–J, M, N), the MC molecule stacks in polar clefts between the paired helical protofilaments that pathologically define AD. Moreover, MC interacts with the local sequence motif PHF6 (Val306 Gln307 Ils308 Val309 Tyr309 Lys311), involved in paired helical filament formation and aggregation (von Bergen et al., 2000). Given that phosphorylation at residues Ser202 and Thr205 is located in a proline-rich region (PRR) and the motif PHF6 is located at the microtubule binding region (MBR) of the protein TAU (Pinzi et al., 2023), it is reasonable to think that MC, upon binding, might induce tridimensional structural changes of the protein, thereby altering the phosphorylation sites and blocking its aggregation (Sonawane et al., 2020). Alternatively, the early anti-amyloid and antioxidant actions of MC might downregulate phosphorylation at TAU Ser202/Thr205. Taken together, these findings suggest that MC might work as a small-molecule inhibitor of TAU aggregation and/or phosphorylation by targeting either monomeric (Kiss et al., 2018; Pickhardt et al., 2015) or TAU fibrils (Seidler et al., 2022) (Fig. 6). MC might serve as a lead molecule for the design of TAU aggregation inhibitors (Wang et al., 2021).

Cell death in AD involves complex pathways (Goel et al., 2022). However, typical apoptosis, involving the activation of several molecules such as c-JUN, TP53, PUMA, and CASP3, has been identified in cortical and hippocampal brain sections from AD patients (Goel et al., 2022; Li, 2021; Wolfrum et al., 2022). We found that MC reduced the phosphorylation of c-JUN (Fig. 7A–H) as well as the expression of TP53 (Fig. 8A–C, G'-J′, K), PUMA (Fig. 8D–F, G''-J″, L), and the activation of the executor CASP3 (Fig. 9A–H), in PSEN1 E280A ChLNs. Therefore, drugs targeting the JNK/p-c-JUNSer63/Ser73, TP53>PUMA > CASP3 pathway (Soto-Mercado et al., 2020) could potentially be useful in the treatment of FAD conditions (e.g., Cho and Hah, 2021; Wójcik et al., 2023; Yarza et al., 2016). Since caspases (Sahoo et al., 2023) and specifically activated executor caspase-3 (CASP3) have been identified in cortical and hippocampal brain sections from AD patients (Stadelmann et al., 1999; Su et al., 2001; Zhang et al., 2022), the pharmacological inhibition of CASP3 could potentially inhibit neuronal loss in cholinergic and hippocampal neurons in FAD. Surprisingly, we found that MC binds with a higher binding affinity to CASP3 (−7.1 kcal/mol) (Fig. 9I and J) than its chemical non-peptide pharmacological inhibitor NSCI (−6.5 kcal/mol) (Fig. 9K and L) according to molecular docking analysis (Fig. 9I–L). Therefore, MC might be a potential inhibitor of CASP3 in PSEN E280A ChLNs. Further cell-free assays, however, are necessary to confirm such assumption.

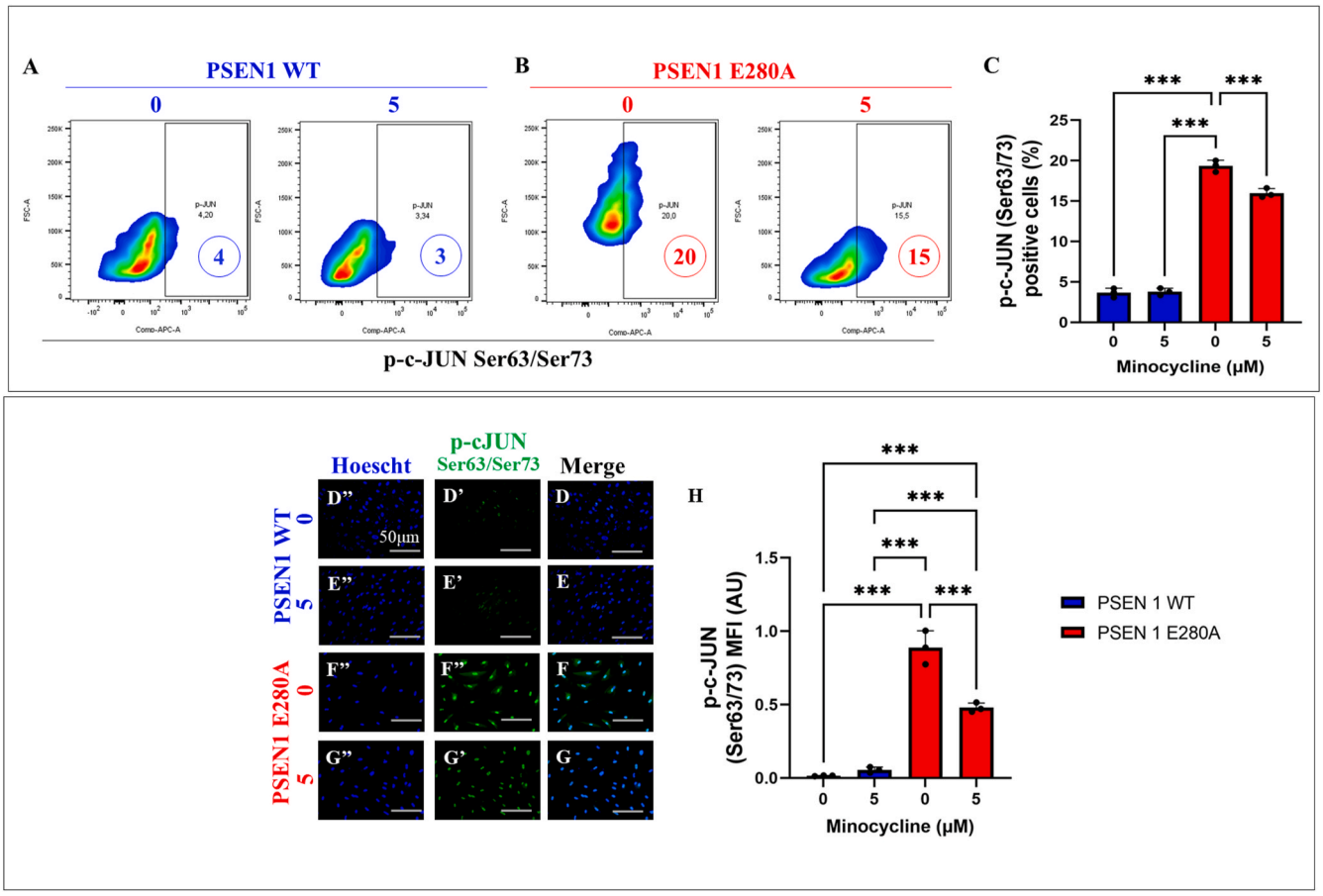

Fig. 7. Minocycline (MC) reduces phosphorylation of JUN (Ser63/Ser73) protein in PSEN1 E280A Cholinergic-like neurons (ChLNs). After 7 days of trans-differentiation, wild-type (WT) PSEN1 and E280A ChLNs were left untreated or treated with MC (5 μM) in regular culture medium (RCm) for 4 days. Flow cytometry (FC) density plots showing the percentage (number in circle) of phosphorylated c-JUN (Ser63/Ser73) in (**A)** WT PSEN1 ChLNs and (**B**) in PSEN1 E280A ChLNs, (**C**) Quantification of the percentage of p-c-JUN (Ser63/Ser73)-positive cells. Representative immunofluorescence merged images (**D-G**) showing WT PSEN1 and PSEN1 E280A ChLNs stained with antibodies against p-c-JUN (Ser63/Ser73). (D′–G′). Nuclei were stained with Hoechst (D″–G″). (**H**) Quantitative data showing the mean fluorescence intensity (MFI) of p-c-JUN (Ser63/Ser73). Density plots and figures represent 1 of 3 independent experiments. Data are expressed as mean ± standard deviation (SD). Significant values were determined by one-way analysis of variance (ANOVA) test with Tukey's post hoc test. Statistical significance: $^{**}p < 0.01$, $^{***}p < 0.001$.

Generally, cholinergic neurons responsive to ACh-induced Ca^{2+} inward flux are considered physiologically functional (Brini et al., 2014). As previously reported (Soto-Mercado et al., 2020), we confirm that PSEN1 E280A ChLNs are irresponsive to ACh-induced Ca^{2+} influx most probably as a result of the high affinity binding between Aβ42 and the α7nAChR (Wang et al., 2000), which are voltage-dependent ion channels (Brown, 2019). Here, we found that MC is capable of restoring ACh-induced Ca^{2+} ion influx in PSEN1 E280A ChLNs (Fig. 10A–D). One possible explanation for this beneficial effect of MC on ChLNs is that MC might restrain, via anti-amyloid interactions, the selective inhibition of the α7-nAChR by Aβ42 (Liu et al., 2001). Whatever the mechanism, MC increased the ACh-induced Ca^{2+} by +92% in mutant ChLNs (Fig. 10E and F). Therefore, MC might work as a neuronal physiological enhancer.

Using PSEN1 E280A ChLNs as an *in vitro* model of FAD offers an unprecedent opportunity to screening for potential new drugs or evaluate repurposed drugs (e.g., MC) before enter clinical trials. Given that PSEN1 E280A ChLNs reproduce the neuropathology of FAD in 11 days (Soto-Mercado et al., 2020), this *in vitro* system become critical for the discover of anti-amyloid, anti-TAU, anti-oxidant, and anti-apoptosis agents in a fast and economical fashion, enabling reliable and efficient drug discovery studies. However, a major drawback of the PSEN1 E280A ChLNs *in vitro* system is its failure to capture the inherent complexity of the patient's brain alterations such as cell-to-cell interactions (e.g., neuron-microglia-astrocytes), loss of memory, disorientation, and behavioral changes, among others (Mendez, 2017). Unfortunately, the lack of a vivo model of FAD PSEN1 E280A has deterred us to evaluate the effect of MC in such a model. Therefore, the creation of a mouse model of FAD bearing the mutation PSEN1 E280A is a topmost priority to advance drug research. Nevertheless, several *in vivo* data suggest that MC might be beneficial for the treatment of FAD. Indeed, it has shown that MC reduced cholinergic dysfunction, modulated the antioxidant status and AChE enzymes, and reduced neuroinflammation-mediated cognitive impairment and amnesia in scopolamine-induced Alzheimer's rat model (Amirahmadi et al., 2022; Eshaghi Ghalibaf et al., 2023). Furthermore, MC improved anxiety-like behavior, recovered Aβ-induced learning and memory deficits, increased GSH and decreased MDA levels, and prevented neuronal loss and the accumulation of Aβ plaques in rats exposed to Aβ (Gholami Mahmoudian et al., 2023). Also, MC reduces inflammatory parameters (e.g., IL-1β, TNF-α, IL-4) in the brain structures (e.g., hippocampus) and serum and reverses memory impairment caused by the administration of amyloid β1-42 in mice (Garcez et al., 2017). We therefore anticipate that MC might ameliorate AD in mice model (Yokoyama et al., 2022).

In conclusion, MC could ameliorate Alzheimer's PSEN1 E280A pathology by interfering with the Aβ-induced cascade of lethal events: **iAβ**≫**H_2O_2**>DJ-1Cys106-SO_3, JNK > **TAU**Ser202/Thr205, TP53, p-c-JUN > PUMA > **CC3**>nuclei fragmentation = apoptosis; and **eAβ**>α7nAChRs (bold indicates MC target). In agreement with *in vivo*

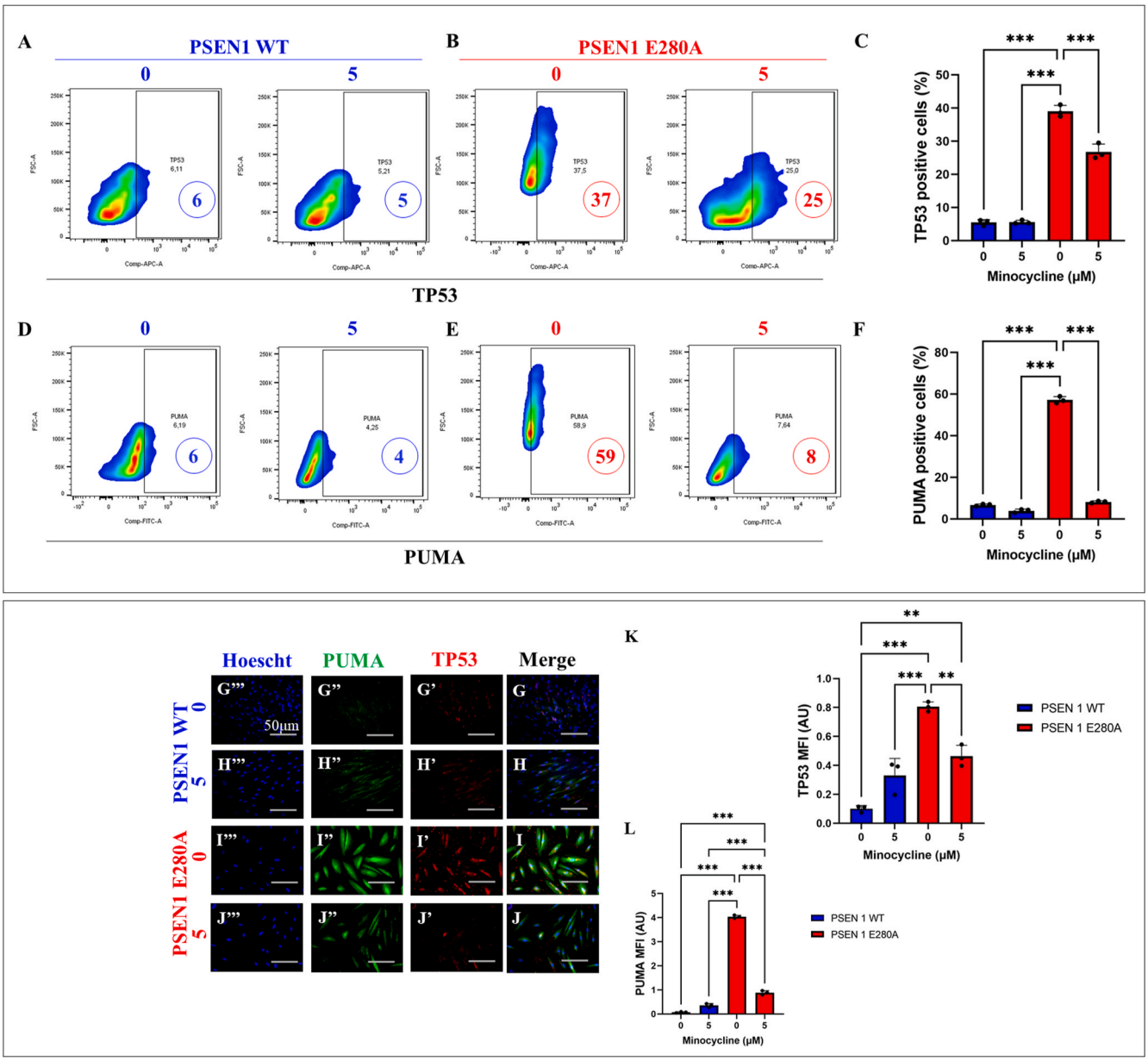

Fig. 8. Minocycline (MC) reduces the cellular presence of TP53 (tumor protein p53) and PUMA (p53 upregulated modulator of apoptosis) protein in PSEN1 E280A Cholinergic-like neurons (ChLNs). After 7 days of transdifferentiation, wild-type (WT) PSEN1 and E280A ChLNs were left untreated or treated with MC (5 μM) in regular culture medium (RCm) for 4 days. Flow cytometry (FC) density plots showing the percentage (number in circle) of TP53 (tumor protein p53) in (**A)** WT PSEN1 ChLNs and (**B**) in PSEN1 E280A ChLNs, (**C**) Quantification of the percentage of TP53-positive cells. FC density plots showing the percentage (number in circle) of PUMA (p53 upregulated modulator of apoptosis) in (**D**) WT PSEN1 ChLNs and (**E**) in PSEN1 E280A ChLNs, (**F**) Quantification of the percentage of PUMA-positive cells. Representative immunofluorescence merged images (**G-J**) showing WT PSEN1 and PSEN1 E280A ChLNs stained with antibodies against PUMA (G′–J′) and TP53 (G″–J″). Nuclei were stained with Hoechst (G‴–J‴). (**K**) Quantitative data showing the MFI of PUMA; (**L**) Quantitative data showing the mean fluorescence intensity (MFI) of TP53. Density plots and figures represent 1 of 3 independent experiments. Data are expressed as mean ± standard deviation (SD). Significant values were determined by one-way analysis of variance (ANOVA) test with Tukey's post hoc test. Statistical significance: **p < 0.01, ***p < 0.001.

data (e.g., Noble et al., 2009), MC might operate as an effective anti-amyloid, anti-TAU, antioxidant, anti-apoptotic, and Ca^{2+} inward facilitator (This work). Overall, MC has the potential to be repurposed as a drug for EOFAD therapy.

Funding

This research was funded by MinCiencias, grant number 1115-844-67062 (contract 830-2019, code 2020-32092) to C.V.-P.

Data availability

The datasets generated and/or analyzed during the current study are included in the manuscript.

Ethics approval

Not applicable.

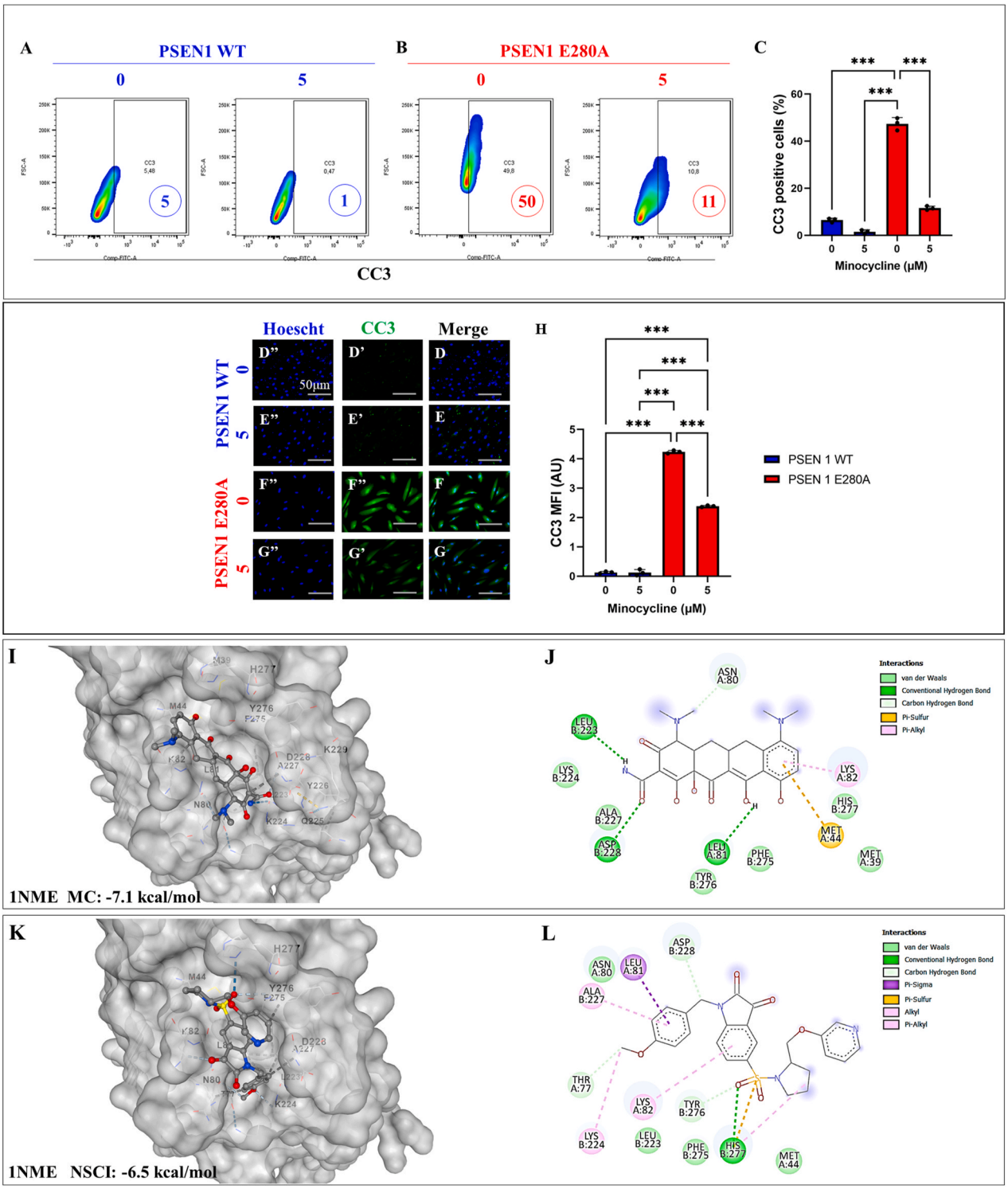

Fig. 9. Minocycline (MC) reduces cleaved caspase 3 (CC3) and binds to caspase 3 (CASP3) in PSEN1 E280A Cholinergic-like neurons (ChLNs). After 7 days of transdifferentiation, wild-type (WT) PSEN1 and E280A ChLNs were left untreated or treated with MC (5 μM) in regular culture medium (RCm) for 4 days. Flow cytometry (FC) density plots showing the percentage (number in circle) of cleaved caspase 3 (CC3) in (**A**) WT PSEN1 ChLNs and (**B**) in PSEN1 E280A ChLNs, (**C**) Quantification of the percentage of CC3-positive cells. Representative immunofluorescence merged images (**D-G**) showing WT PSEN1 and PSEN1 E280A ChLNs stained with antibodies against CC3 (D′–G′). Nuclei were stained with Hoechst (D″–G″). (**H**) Quantitative data showing the mean fluorescence intensity (MFI) of CC3. Density plots and figures represent 1 of 3 independent experiments. Data are expressed as mean ± standard deviation (SD). Significant values were determined by one-way analysis of variance (ANOVA) test with Tukey's post hoc test. Statistical significance: ***$p < 0.001$. (**I**) Representative CB-Dock2 3D image showing the molecular docking of caspase 3 (CASP3, PDB ID: 1NME) with MC (CID: 54675783); (**J**) 2D diagram showing conventional hydrogen bond between monomeric CASP3-MC interaction, (**K**) Representative CB-Dock2 3D image showing the molecular docking of CASP3 with NSCI (CID: 11591540), (**L**) 2D diagram showing conventional hydrogen bond between CASP3-NSCI interaction.

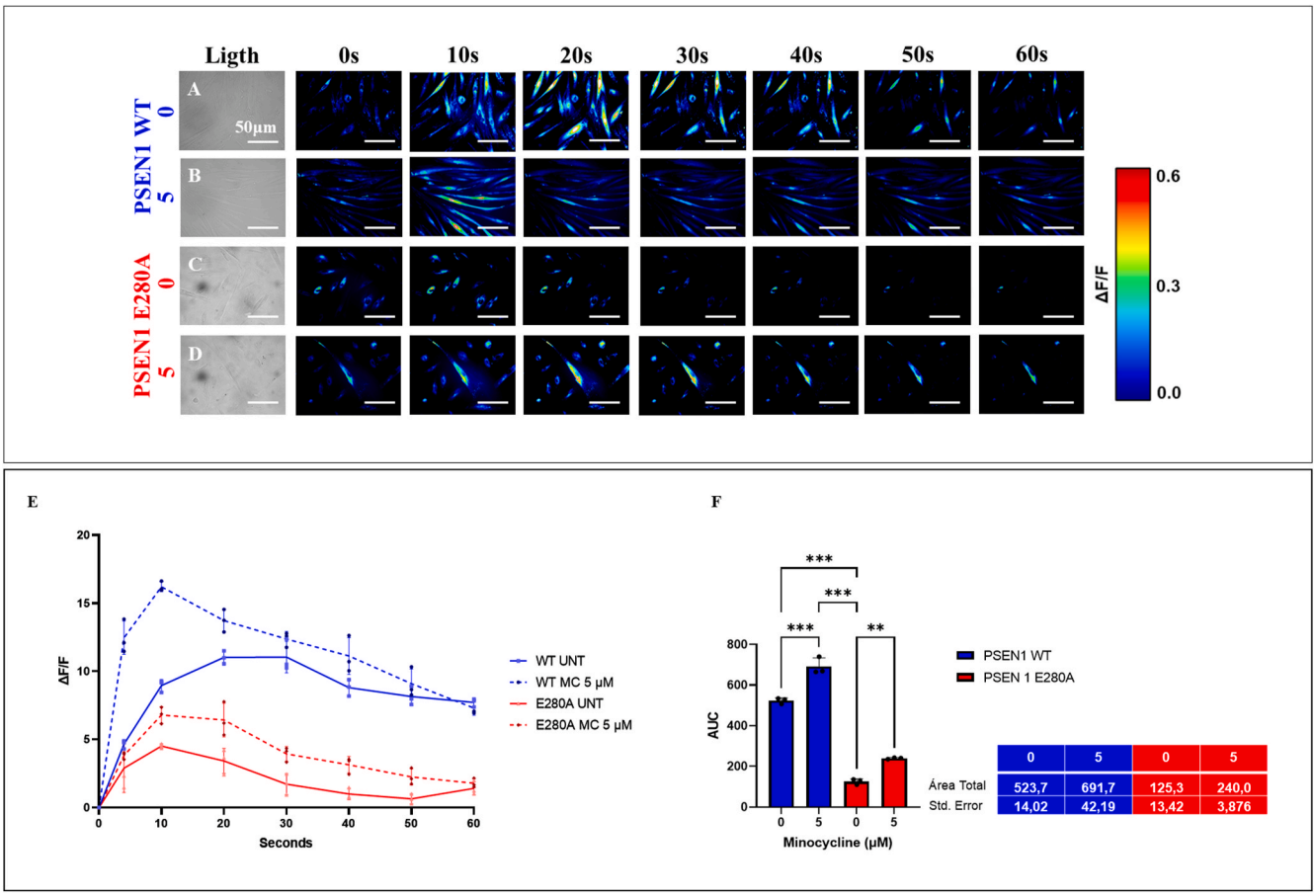

Fig. 10. Minocycline (MC) restores Ca^{2+} dysregulation in PSEN1 E280A Cholinergic-like neurons (ChLNs). After 7 days of transdifferentiation, wild-type (WT) PSEN1 and E280A ChLNs were left untreated or treated with MC (5 μM) in regular culture medium (RCm) for 4 days. (**A–D**) Time-lapse images (0, 10, 20, 30, 40, 50, and 60 s) of Ca^{2+} fluorescence in PSEN1 WT (A, B) and E280A ChLNs (C, D) in response to ACh treatment. ACh was added to the culture at 0 s (arrow), and Ca^{2+} fluorescence of cells was monitored at the indicated times. The color contrast indicates fluorescence intensity: dark blue < light blue < green < yellow < red. (**E**) Normalized mean fluorescence signal (ΔF/F) over time from cells indicating temporally elevated cytoplasmic Ca^{2+} in response to ACh treatment; (**F**) Calculated area under the curve (AUC). Figures represent 1 of 3 independent experiments. Data are expressed as mean ± standard deviation (SD). Significant values were determined by one-way analysis of variance (ANOVA) test with Tukey's post hoc test. Statistical significance: ***p < 0.001.

Consent to participate

Not applicable.

Consent for publication

Not applicable.

CRediT authorship contribution statement

Daniela Giraldo-Berrio: Writing – review & editing, Validation, Investigation, Formal analysis, Data curation. **Marlene Jimenez-Del-Rio:** Writing – review & editing, Writing – original draft, Supervision, Resources, Project administration, Investigation, Funding acquisition, Conceptualization. **Carlos Velez-Pardo:** Writing – review & editing, Writing – original draft, Visualization, Validation, Resources, Methodology, Investigation, Funding acquisition, Conceptualization.

Declaration of competing interest

The authors declare that they have no known competing financial interests or personal relationships that could have appeared to influence the work reported in this paper.

Data availability

No data was used for the research described in the article.

Acknowledgements

Not applicable.

References

Acosta-Baena, N., Sepulveda-Falla, D., Lopera-Gómez, C.M., Jaramillo-Elorza, M.C., Moreno, S., Aguirre-Acevedo, D.C., Saldarriaga, A., Lopera, F., 2011. Pre-dementia clinical stages in presenilin 1 E280A familial early-onset Alzheimer's disease: a retrospective cohort study. Lancet Neurol. 10, 213–220. https://doi.org/10.1016/S1474-4422(10)70323-9.

Adan, A., Alizada, G., Kiraz, Y., Baran, Y., Nalbant, A., 2017. Flow cytometry: basic principles and applications. Crit. Rev. Biotechnol. 37, 163–176. https://doi.org/10.3109/07388551.2015.1128876.

Amirahmadi, S., Farimani, F.D., Akbarian, M., Mirzavi, F., Eshaghi Ghalibaf, M.H., Rajabian, A., Hosseini, M., 2022. Minocycline attenuates cholinergic dysfunction and neuro-inflammation-mediated cognitive impairment in scopolamine-induced Alzheimer's rat model. Inflammopharmacology 30, 2385–2397. https://doi.org/10.1007/s10787-022-01071-2.

Anderson, C., Bucholc, M., McClean, P.L., Zhang, S.-D., 2023. The potential of a stratified approach to drug repurposing in Alzheimer's disease. Biomolecules 14, 11. https://doi.org/10.3390/biom14010011.

Andrich, K., Bieschke, J., 2015. The effect of (-)-Epigallo-catechin-(3)-gallate on amyloidogenic proteins suggests a common mechanism. Adv. Exp. Med. Biol. 863, 139–161. https://doi-org.udea.lookproxy.com/10.1007/978-3-319-18365-7_7.

Bravo, K., Quintero, C., Agudelo, C., García, S., Bríñez, A., Osorio, E., 2020. CosIng database analysis and experimental studies to promote Latin American plant biodiversity for cosmetic use. Ind. Crops Prod. 144, 112007 https://doi.org/10.1016/j.indcrop.2019.112007.

Brini, M., Calì, T., Ottolini, D., Carafoli, E., 2014. Neuronal calcium signaling: function and dysfunction. Cell. Mol. Life Sci. 71, 2787–2814. https://doi.org/10.1007/s00018-013-1550-7.

Brogden, R.N., Speight, T.M., Avery, G.S., 1975. Minocycline: a review of its antibacterial and pharmacokinetic properties and therapeutic use. Drugs 9, 251–291. https://doi.org/10.2165/00003495-197509040-00005.

Brown, D.A., 2019. Acetylcholine and cholinergic receptors. Brain Neurosci. Adv. 3, 239821281882050 https://doi.org/10.1177/2398212818820506.

Cho, H., Hah, J.-M., 2021. A perspective on the development of c-Jun N-terminal kinase inhibitors as therapeutics for Alzheimer's disease: investigating structure through docking studies. Biomedicines 9, 1431. https://doi.org/10.3390/biomedicines9101431.

Chen-Roetling, J., Chen, L., Regan, R.F., 2009. Minocycline attenuates iron neurotoxicity in cortical cell cultures. Biochem. Biophys. Res. Commun. 386, 322–326. https://doi-org.udea.lookproxy.com/10.1016/j.bbrc.2009.06.026.

Chu, W., Zhang, J., Zeng, C., Rothfuss, J., Tu, Z., Chu, Y., Reichert, D.E., Welch, M.J., Mach, R.H., 2005. Benzylisatin sulfonamide analogues as potent caspase-3 inhibitors: synthesis, in vitro activity, and molecular modeling studies. J. Med. Chem. 48, 7637–7647. https://doi.org/10.1021/jm0506625.

Costigan, A., Hollville, E., Martin, S.J., 2023. Discriminating between apoptosis, necrosis, necroptosis, and ferroptosis by microscopy and flow cytometry. Curr. Protoc. 3, e951 https://doi.org/10.1002/cpz1.951.

Dinkel, F., Trujillo-Rodriguez, D., Villegas, A., Streffer, J., Mercken, M., Lopera, F., Glatzel, M., Sepulveda-Falla, D., 2020. Decreased deposition of beta-amyloid 1-38 and increased deposition of beta-amyloid 1-42 in brain tissue of presenilin-1 E280A familial Alzheimer's disease patients. Front. Aging Neurosci. 12, 220. https://doi.org/10.3389/fnagi.2020.00220.

Doig, A.J., Derreumaux, P., 2015. Inhibition of protein aggregation and amyloid formation by small molecules. Curr. Opin. Struct. Biol. 30, 50–56. https://doi.org/10.1016/j.sbi.2014.12.004.

Eshaghi Ghalibaf, M.H., Rajabian, A., Parviz, M., Akbarian, M., Amirahmadi, S., Vafaee, F., Hosseini, M., 2023. Minocycline alleviated scopolamine-induced amnesia by regulating antioxidant and cholinergic function. Heliyon 9, e13452. https://doi-org.udea.lookproxy.com/10.1016/j.heliyon.2023.e13452.

Familian, A., Boshuizen, R.S., Eikelenboom, P., Veerhuis, R., 2006. Inhibitory effect of minocycline on amyloid β fibril formation and human microglial activation. Glia 53, 233–240. https://doi.org/10.1002/glia.20268.

Fang, M., Zhang, Q., Wang, X., Su, K., Guan, P., Hu, X., 2022. Inhibition mechanisms of (−)-Epigallocatechin-3-gallate and genistein on amyloid-beta 42 peptide of Alzheimer's disease via molecular simulations. ACS Omega 7, 19665–19675. https://doi.org/10.1021/acsomega.2c01412.

Ferretti, M.T., Allard, S., Partridge, V., Ducatenzeiler, A., Cuello, A.C., 2012. Minocycline corrects early, pre-plaque neuroinflammation and inhibits BACE-1 in a transgenic model of Alzheimer's disease-like amyloid pathology. J. Neuroinflammation 9, 62. https://doi.org/10.1186/1742-2094-9-62.

Firouzi, R., Sowlati-Hashjin, S., Chávez-García, C., Ashouri, M., Karimi-Jafari, M.H., Karttunen, M., 2023. Identification of catechins' binding sites in monomeric Aβ42 through ensemble docking and MD simulations. Int. J. Mol. Sci. 24, 8161. https://doi.org/10.3390/ijms24098161.

Flamm, R.K., Shortridge, D., Castanheira, M., Sader, H.S., Pfaller, M.A., 2019. In vitro activity of minocycline against U.S. Isolates of acinetobacter baumannii-acinetobacter calcoaceticus species complex, stenotrophomonas maltophilia, and burkholderia cepacia complex: results from the SENTRY antimicrobial surveillance program, 2014 to 2018. Antimicrob. Agents Chemother. 63, e01154 https://doi.org/10.1128/AAC.01154-19, 19.

Frederiksen, H.R., Holst, B., Mau-Holzmann, U.A., Freude, K., Schmid, B., 2019. Generation of two isogenic iPSC lines with either a heterozygous or a homozygous E280A mutation in the PSEN1 gene. Stem Cell Res. 35, 101403 https://doi.org/10.1016/j.scr.2019.101403.

Garcez, M.L., Mina, F., Bellettini-Santos, T., Carneiro, F.G., Luz, A.P., Schiavo, G.L., Andrighetti, M.S., Scheid, M.G., Bolfe, R.P., Budni, J., 2017. Minocycline reduces inflammatory parameters in the brain structures and serum and reverses memory impairment caused by the administration of amyloid β (1-42) in mice. Prog. Neuro-Psychopharmacol. Biol. Psychiatry 77, 23–31. https://doi.org/10.1016/j.pnpbp.2017.03.010.

Garrido-Mesa, N., Zarzuelo, A., Gálvez, J., 2013a. Minocycline: far beyond an antibiotic. Br. J. Pharmacol. 169, 337–352. https://doi-org.udea.lookproxy.com/10.1111/bph.12139.

Garrido-Mesa, N., Zarzuelo, A., Gálvez, J., 2013b. What is behind the non-antibiotic properties of minocycline? Pharmacol. Res. 67, 18–30. https://doi-org.udea.lookproxy.com/10.1016/j.phrs.2012.10.006.

Gholami Mahmoudian, Z., Ghanbari, A., Rashidi, I., Amiri, I., Komaki, A., 2023. Minocycline effects on memory and learning impairment in the beta-amyloid-induced Alzheimer's disease model in male rats using behavioral, biochemical, and histological methods. Eur. J. Pharmacol. 953, 175784 https://doi.org/10.1016/j.ejphar.2023.175784.

Goel, P., Chakrabarti, S., Goel, K., Bhutani, K., Chopra, T., Bali, S., 2022. Neuronal cell death mechanisms in Alzheimer's disease: an insight. Front. Mol. Neurosci. 15, 937133 https://doi.org/10.3389/fnmol.2022.937133.

Grabowska, M.E., Huang, A., Wen, Z., Li, B., Wei, W.-Q., 2023. Drug repurposing for Alzheimer's disease from 2012–2022—a 10-year literature review. Front. Pharmacol. 14, 1257700 https://doi.org/10.3389/fphar.2023.1257700.

Griffin, M.O., Ceballos, G., Villarreal, F.J., 2011. Tetracycline compounds with non-antimicrobial organ protective properties: possible mechanisms of action. Pharmacol. Res. 63, 102–107. https://doi-org.udea.lookproxy.com/10.1016/j.phrs.2010.10.004.

Guéroux, M., Fleau, C., Slozeck, M., Laguerre, M., Pianet, I., 2017. Epigallocatechin 3-gallate as an inhibitor of tau phosphorylation and aggregation: a molecular and structural insight. J. Prevent. Alzheimer's Dise. 4, 218–225. https://doi.org/10.14283/jpad.2017.35.

Hiroaki, H., 2023. Molecular mechanisms of amyloid-β peptide fibril and oligomer formation: NMR-based challenges. Biophys. Physicobiol. 20, e200007 https://doi.org/10.2142/biophysico.bppb-v20.0007.

Hollville, E., Martin, S.J., 2016. Measuring apoptosis by microscopy and flow cytometry. Curr. Protoc. Im. 112 (14.38) https://doi.org/10.1002/0471142735.im1438s112, 1-14.38.24.

Howard, R., Zubko, O., Gray, R., Bradley, R., Harper, E., Kelly, L., Pank, L., O'Brien, J., Fox, C., Tabet, N., Livingston, G., Bentham, P., McShane, R., Burns, A., Ritchie, C., Reeves, S., Lovestone, S., Ballard, C., Noble, W., Wilcock, G., Nilforooshan, R., 2020. Minocycline 200 mg or 400 mg versus placebo for mild Alzheimer's disease: the MADE Phase II, three-arm RCT. Efficacy Mech. Eval. 7, 1–62. https://doi.org/10.3310/eme07020.

Jänicke, R.U., Sprengart, M.L., Wati, M.R., Porter, A.G., 1998. Caspase-3 is required for DNA fragmentation and morphological changes associated with apoptosis. J. Biol. Chem. 273, 9357–9360. https://doi.org/10.1074/jbc.273.16.9357.

Kapoor, M.P., Sugita, M., Fukuzawa, Y., Okubo, T., 2017. Physiological effects of epigallocatechin-3-gallate (EGCG) on energy expenditure for prospective fat oxidation in humans: a systematic review and meta-analysis. J. Nutr. Biochem. 43, 1–10. https://doi.org/10.1016/j.jnutbio.2016.10.013.

Kinumi, T., Kimata, J., Taira, T., Ariga, H., Niki, E., 2004. Cysteine-106 of DJ-1 is the most sensitive cysteine residue to hydrogen peroxide-mediated oxidation *in vivo* in human umbilical vein endothelial cells. Biochem. Biophys. Res. Commun. 317, 722–728. https://doi.org/10.1016/j.bbrc.2004.03.110.

Kiss, R., Csizmadia, G., Solti, K., Keresztes, A., Zhu, M., Pickhardt, M., Mandelkow, E., Tóth, G., 2018. Structural basis of small molecule targetability of monomeric tau protein. ACS Chem. Neurosci. 9, 2997–3006. https://doi.org/10.1021/acschemneuro.8b00182.

Kładna, A., Michalska, T., Berczyński, P., Kruk, I., Aboul-Enein, H.Y., 2012. Evaluation of the antioxidant activity of tetracycline antibiotics *in vitro*. Luminescence 27, 249–255. https://doi.org/10.1002/bio.1339.

Kraus, R.L., Pasieczny, R., Lariosa-Willingham, K., Turner, M.S., Jiang, A., Trauger, J.W., 2005. Antioxidant properties of minocycline: neuroprotection in an oxidative stress assay and direct radical-scavenging activity. J. Neurochem. 94, 819–827. https://doi.org/10.1111/j.1471-4159.2005.03219.x.

Lalli, M.A., Cox, H.C., Arcila, M.L., Cadavid, L., Moreno, S., Garcia, G., Madrigal, L., Reiman, E.M., Arcos-Burgos, M., Bedoya, G., Brunkow, M.E., Glusman, G., Roach, J. C., Hood, L., Kosik, K.S., Lopera, F., 2014. Origin of the PSEN1 E280A mutation causing early-onset Alzheimer's disease. Alzheimer's Dementia 10, S277–S283.e10. https://doi.org/10.1016/j.jalz.2013.09.005.

Lauritzen, I., Pardossi-Piquard, R., Bourgeois, A., Bécot, A., Checler, F., 2019. Does intraneuronal accumulation of carboxyl-terminal fragments of the amyloid precursor protein trigger early neurotoxicity in Alzheimer's disease? Curr. Alzheimer Res. 16, 453–457. https://doi.org/10.2174/1567205016666190325092841.

Lazic, S.E., Clarke-Williams, C.J., Munafò, M.R., 2018. What exactly is 'N' in cell culture and animal experiments? PLoS Biol. 16, e2005282 https://doi.org/10.1371/journal.pbio.2005282.

Legeay, S., Rodier, M., Fillon, L., Faure, S., Clere, N., 2015. Epigallocatechin gallate: a review of its beneficial properties to prevent metabolic syndrome. Nutrients 7, 5443–5468. https://doi.org/10.3390/nu7075230.

Li, M., 2021. The role of P53 up-regulated modulator of apoptosis (PUMA) in ovarian development, cardiovascular and neurodegenerative diseases. Apoptosis 26, 235–247. https://doi.org/10.1007/s10495-021-01667-z.

Liu, A.K.L., Chang, R.C.-C., Pearce, R.K.B., Gentleman, S.M., 2015. Nucleus basalis of Meynert revisited: anatomy, history and differential involvement in Alzheimer's and Parkinson's disease. Acta Neuropathol. 129, 527–540. https://doi.org/10.1007/s00401-015-1392-5.

Liu, Q., Kawai, H., Berg, D.K., 2001. β-Amyloid peptide blocks the response of α7-containing nicotinic receptors on hippocampal neurons. Proc. Natl. Acad. Sci. USA 98, 4734–4739. https://doi.org/10.1073/pnas.081553598.

Liu, Y., Yang, X., Gan, J., Chen, S., Xiao, Z.-X., Cao, Y., 2022. CB-Dock2: improved protein–ligand blind docking by integrating cavity detection, docking and homologous template fitting. Nucleic Acids Res. 50, W159–W164. https://doi.org/10.1093/nar/gkac394.

Lopera, F., 1997. Clinical features of early-onset Alzheimer disease in a large kindred with an E280A presenilin-1 mutation. JAMA, J. Am. Med. Assoc. 277, 793. https://doi.org/10.1001/jama.1997.03540340027028.

Macdonald, H., Kelly, R.G., Allen, E.S., Noble, J.F., Kanegis, L.A., 1973. Pharmacokinetic studies on minocycline in man. Clin. Pharmacol. Therapeut. 14, 852–861. https://doi-org.udea.lookproxy.com/10.1002/cpt1973145852.

Mendez, M.F., 2017. Early-onset Alzheimer disease. Neurol. Clin. 35, 263–281. https://doi.org/10.1016/j.ncl.2017.01.005.

Mendivil-Perez, M., Velez-Pardo, C., Jimenez-Del-Rio, M., 2019. Direct transdifferentiation of human Wharton's jelly mesenchymal stromal cells into cholinergic-like neurons. J. Neurosci. Methods 312, 126–138. https://doi.org/10.1016/j.jneumeth.2018.11.019.

Mendivil-Perez, M., Velez-Pardo, C., Lopera, F., Kosik, K.S., Jimenez-Del-Rio, M., 2023. PSEN1 E280A cholinergic-like neurons and cerebral spheroids derived from mesenchymal stromal cells and from induced pluripotent stem cells are

neuropathologically equivalent. Int. J. Mol. Sci. 24, 8957. https://doi.org/10.3390/ijms24108957.
Nagle, D.G., Ferreira, D., Zhou, Y.D., 2006. Epigallocatechin-3-gallate (EGCG): chemical and biomedical perspectives. Phytochemistry 67, 1849–1855. https://doi.org/10.1016/j.phytochem.2006.06.020.
Ngo, S.T., Truong, D.T., Tam, N.M., Nguyen, M.T., 2017. EGCG inhibits the oligomerization of amyloid beta (16-22) hexamer: theoretical studies. J. Mol. Graph. Model. 76, 1–10. https://doi.org/10.1016/j.jmgm.2017.06.018.
Noble, W., Garwood, C., Stephenson, J., Kinsey, A.M., Hanger, D.P., Anderton, B.H., 2009. Minocycline reduces the development of abnormal tau species in models of Alzheimer's disease. Faseb. J. 23, 739–750. https://doi.org/10.1096/fj.08-113795.
Padhi, D., Govindaraju, T., 2022. Mechanistic insights for drug repurposing and the design of hybrid drugs for Alzheimer's disease. J. Med. Chem. 65, 7088–7105. https://doi.org/10.1021/acs.jmedchem.2c00335.
Pap, P., Kőszeghy, Á., Szűcs, G., Rusznák, Z., 2009. Cytoplasmic Ca2+ concentration changes evoked by cholinergic stimulation in primary astrocyte cultures prepared from the rat cochlear nucleus. Hear. Res. 255, 73–83. https://doi.org/10.1016/j.heares.2009.05.006.
Pickhardt, M., Neumann, T., Schwizer, D., Callaway, K., Vendruscolo, M., Schenk, D., St George-Hyslop, P., Mandelkow, E.M., Dobson, C.M., McConlogue, L., Mandelkow, E., Tóth, G., 2015. Identification of small molecule inhibitors of tau aggregation by target-ing monomeric tau as a potential therapeutic approach for tauopathies. Curr. Alzheimer Res. 12, 814–828.
Pinzi, L., Bisi, N., Sorbi, C., Franchini, S., Tonali, N., Rastelli, G., 2023. Insights into the structural conformations of the tau protein in different aggregation status. Molecules 28, 4544. https://doi.org/10.3390/molecules28114544.
Reiman, E.M., Pruzin, J.J., Rios-Romenets, S., Brown, C., Giraldo, M., Acosta-Baena, N., Tobon, C., Hu, N., Chen, Y., Ghisays, V., Enos, J., Goradia, D.D., Lee, W., Luo, J., Malek-Ahmadi, M., Protas, H., Thomas, R.G., Chen, K., Su, Y., Boker, C., Mastroeni, D., Alvarez, S., Quiroz, Y.T., Langbaum, J.B., Sink, K.M., Lopera, F., Tariot, P.N., 2023. A public resource of baseline data from the Alzheimer's prevention initiative autosomal-dominant Alzheimer's disease trial. Alzheimer's Dementia 19, 1938–1946. https://doi.org/10.1002/alz.12843.
Sahoo, G., Samal, D., Khandayataray, P., Murthy, M.K., 2023. A review on caspases: key regulators of biological activities and apoptosis. Mol. Neurobiol. 60, 5805–5837. https://doi.org/10.1007/s12035-023-03433-5.
Santoro, A., Grimaldi, M., Buonocore, M., Stillitano, I., D'Ursi, A.M., 2021. Exploring the early stages of the amyloid Aβ(1–42) peptide aggregation process: an NMR study. Pharmaceuticals 14, 732. https://doi.org/10.3390/ph14080732.
Sawaya, M.R., Sambashivan, S., Nelson, R., Ivanova, M.I., Sievers, S.A., Apostol, M.I., Thompson, M.J., Balbirnie, M., Wiltzius, J.J.W., McFarlane, H.T., Madsen, A.Ø., Riekel, C., Eisenberg, D., 2007. Atomic structures of amyloid cross-β spines reveal varied steric zippers. Nature 447, 453–457. https://doi.org/10.1038/nature05695.
Schildknecht, S., Pape, R., Müller, N., Robotta, M., Marquardt, A., Bürkle, A., Drescher, M., Leist, M., 2011. Neuroprotection by minocycline caused by direct and specific scavenging of peroxynitrite. J. Biol. Chem. 286, 4991–5002. https://doi-org.udea.lookproxy.com/10.1074/jbc.M110.169565.
Seidler, P.M., Murray, K.A., Boyer, D.R., Ge, P., Sawaya, M.R., Hu, C.J., Cheng, X., Abskharon, R., Pan, H., DeTure, M.A., Williams, C.K., Dickson, D.W., Vinters, H.V., Eisenberg, D.S., 2022. Structure-based discovery of small molecules that disaggregate Alzheimer's disease tissue derived tau fibrils *in vitro*. Nat. Commun. 13, 5451. https://doi.org/10.1038/s41467-022-32951-4.
Sekiguchi-Tonosaki, M., Obata, M., Haruki, A., Himi, T., Kosaka, J., 2009. Acetylcholine induces Ca 2+signaling in chicken retinal pigmented epithelial cells during dedifferentiation. Am. J. Physiol. Cell Physiol. 296, C1195–C1206. https://doi.org/10.1152/ajpcell.00423.2008.
Shortridge, D., Arends, S.J.R., Streit, J.M., Castanheira, M., 2021. Minocycline activity against unusual clinically significant gram-negative pathogens. Antimicrob. Agents Chemother. 65, e0126421 https://doi.org/10.1128/AAC.01264-21.
Sonawane, S.K., Chidambaram, H., Boral, D., Gorantla, N.V., Balmik, A.A., Dangi, A., Ramasamy, S., Marelli, U.K., Chinnathambi, S., 2020. EGCG impedes human Tau aggregation and interacts with Tau. Sci. Rep. 10, 12579 https://doi.org/10.1038/s41598-020-69429-6.
Song, H., Wang, Q., He, A., Li, S., Guan, X., Hu, Y., Feng, S., 2022. Antioxidant activity, storage stability and *in vitro* release of epigallocatechin-3-gallate (EGCG) encapsulated in hordein nanoparticles. Food Chem. 388, 132903 https://doi.org/10.1016/j.foodchem.2022.132903.
Soto-Mercado, V., Mendivil-Perez, M., Velez-Pardo, C., Lopera, F., Jimenez-Del-Rio, M., 2020. Cholinergic-like neurons carrying PSEN1 E280A mutation from familial Alzheimer's disease reveal intraneuronal sAPPβ fragments accumulation, hyperphosphorylation of TAU, oxidative stress, apoptosis and Ca2+ dysregulation: therapeutic implications. PLoS One 15, e0221669. https://doi.org/10.1371/journal.pone.0221669.
Soto-Mercado, V., Mendivil-Perez, M., Velez-Pardo, C., Jimenez-Del-Rio, M., 2021. (-)-Epigallocatechin-3-Gallate diminishes intra-and extracellular amyloid-induced cytotoxic effects on cholinergic-like neurons from familial Alzheimer's disease PSEN1 E280A. Biomolecules 11, 1845. https://doi-org.udea.lookproxy.com/10.3390/biom11121845.
Soto-Mercado, V., Mendivil-Perez, M., Velez-Pardo, C., Jimenez-Del-Rio, M., 2024. Neuroprotective effect of combined treatment with epigallocatechin 3-gallate and melatonin on familial Alzheimer's disease PSEN1 E280A cerebral spheroids derived from menstrual mesenchymal stromal cells. J. Alzheim. Dis.: JAD 99 (s1), S51–S66. https://doi-org.udea.lookproxy.com/10.3233/JAD-220903.
Stadelmann, C., Deckwerth, T.L., Srinivasan, A., Bancher, C., Brück, W., Jellinger, K., Lassmann, H., 1999. Activation of caspase-3 in single neurons and autophagic granules of granulovacuolar degeneration in Alzheimer's disease. Am. J. Pathol. 155, 1459–1466. https://doi.org/10.1016/S0002-9440(10)65460-0.
Su, J.H., Zhao, M., Anderson, A.J., Srinivasan, A., Cotman, C.W., 2001. Activated caspase-3 expression in Alzheimer's and aged control brain: correlation with Alzheimer pathology. Brain Res. 898, 350–357. https://doi.org/10.1016/S0006-8993(01)02018-2.
Takahashi, R.H., Nagao, T., Gouras, G.K., 2017. Plaque formation and the intraneuronal accumulation of β-amyloid in Alzheimer's disease. Pathol. Int. 67, 185–193. https://doi.org/10.1111/pin.12520.
Takasugi, N., Komai, M., Kaneshiro, N., Ikeda, A., Kamikubo, Y., Uehara, T., 2023. The pursuit of the "inside" of the amyloid hypothesis—is C99 a promising therapeutic target for Alzheimer's disease? Cells 12, 454. https://doi.org/10.3390/cells12030454.
Teipel, S., Grazia, A., Dyrba, M., Grothe, M.J., Pomara, N., 2024. Basal forebrain volume and metabolism in carriers of the Colombian mutation for autosomal dominant Alzheimer's disease. Sci. Rep. 14, 11268 https://doi.org/10.1038/s41598-024-60799-9.
Trejo-Lopez, J.A., Yachnis, A.T., Prokop, S., 2022. Neuropathology of Alzheimer's disease. Neurotherapeutics 19, 173–185. https://doi.org/10.1007/s13311-021-01146-y.
Vallejo-Diez, S., Fleischer, A., Martín-Fernández, J.M., Sánchez-Gilabert, A., Castresana, M., Aguillón, D., Villegas, A., Mastronardi, C.A., Espinosa, L.G., Arcos-Burgos, M., del Pozo, Á., Herrán, E., Gainza, E., Isaza-Ruget, M., Lopera, F., Bachiller, D., 2019. Generation of one iPSC line (IMEDEAi006-A) from an early-onset familial Alzheimer's Disease (fAD) patient carrying the E280A mutation in the PSEN1 gene. Stem Cell Res. 37, 101440 https://doi.org/10.1016/j.scr.2019.101440.
Volloch, V., Rits-Volloch, S., 2023a. The amyloid cascade hypothesis 2.0: generalization of the concept. J. Alzheimers Dis. Rep. 7, 21–35. https://doi.org/10.3233/ADR-220079.
Volloch, V., Rits-Volloch, S., 2023b. Effect of lecanemab and donanemab in early Alzheimer's disease: mechanistic interpretation in the amyloid cascade hypothesis 2.0 perspective. J. Alzheim. Dis. 93, 1277–1284. https://doi.org/10.3233/JAD-230164.
von Bergen, M., Friedhoff, P., Biernat, J., Heberle, J., Mandelkow, E.-M., Mandelkow, E., 2000. Assembly of τ protein into Alzheimer paired helical filaments depends on a local sequence motif (306VQIVYK 311) forming β structure. Proc. Natl. Acad. Sci. USA 97, 5129–5134. https://doi.org/10.1073/pnas.97.10.5129.
Wang, D., Huang, X., Yan, L., Zhou, L., Yan, C., Wu, J., Su, Z., Huang, Y., 2021. The structure biology of tau and clue for aggregation inhibitor design. Protein J. 40, 656–668. https://doi.org/10.1007/s10930-021-10017-6.
Wang, H.Y., Lee, D.H., D'Andrea, M.R., Peterson, P.A., Shank, R.P., Reitz, A.B., 2000. beta-Amyloid(1-42) binds to alpha7 nicotinic acetylcholine receptor with high affinity. Implications for Alzheimer's disease pathology. J. Biol. Chem. 275, 5626–5632. https://doi.org/10.1074/jbc.275.8.5626.
Wójcik, P., Jastrzębski, M.K., Zięba, A., Matosiuk, D., Kaczor, A.A., 2023. Caspases in Alzheimer's disease: mechanism of activation, role, and potential treatment. Mol. Neurobiol. 61, 4834–4853. https://doi.org/10.1007/s12035-023-03847-1.
Wolfrum, P., Fietz, A., Schnichels, S., Hurst, J., 2022. The function of p53 and its role in Alzheimer's and Parkinson's disease compared to age-related macular degeneration. Front. Neurosci. 16, 1029473 https://doi.org/10.3389/fnins.2022.1029473.
Yarza, R., Vela, S., Solas, M., Ramirez, M.J., 2016. c-Jun N-terminal kinase (JNK) signaling as a therapeutic target for Alzheimer's disease. Front. Pharmacol. 6, 321. https://doi.org/10.3389/fphar.2015.00321.
Yokoyama, M., Kobayashi, H., Tatsumi, L., Tomita, T., 2022. Mouse models of Alzheimer's disease. Front. Mol. Neurosci. 15, 912995. https://doi-org.udea.lookproxy.com/10.3389/fnmol.2022.912995.
Zhang, P., Zhang, M., Mellich, T.A., Pearson, B.J., Chen, J., Zhang, Z., 2022. Variation in rotenone and deguelin contents among strains across four Tephrosia species and their activities against aphids and whiteflies. Toxins 14, 339. https://doi.org/10.3390/toxins14050339.
Zhao, Y., Wang, C., He, W., Cai, Z., 2022. Ameliorating Alzheimer's-like pathology by minocycline via inhibiting Cdk5/p25 signaling. Curr. Neuropharmacol. 20, 1783–1792. https://doi.org/10.2174/1570159X19666211202124925.